Weidling *et al.*
Acta Neuropathologica Communications (2025) 13:108
https://doi.org/10.1186/s40478-025-02000-4

Acta Neuropathologica Communications

RESEARCH

Open Access

hiPSC-neurons recapitulate the subtype-specific cell intrinsic nature of susceptibility to neurodegenerative disease-relevant aggregation

Ian Weidling[1†], Christina N. Preiss[1], Sarah E. Chancellor[1], Gyan Srivastava[1†], Lauren Gibilisco[1], Gen Lin[2], Melanie Shackett Brennan[1], Janice Lee[1], Lindsay M. Roth[1], Olga Morozova[1], Kyong Nyon Nam[1], Nehal R. Patel[1], Qing Liu[1], J. K. Thomas[3†], Peter Reinhardt[4], Ruven Wilkens[4], Dagmar E. Ehrnhoefer[4], Andreas Striebinger[4], Stefan Barghorn[4], Christina Xanthopoulos[4], Marie-Theres Weil[4†], Sandra Biesinger[4], Miroslav Cik[4], Nandini Romanul[1], Kiran Yanamandra[1], Alessandra M. Welker[1], Jessica Wu[1], Laura Gasparini[4], Jan Stöhr[1], Xavier Langlois[1] and Justine D. Manos[1*]

Abstract

Alzheimer's disease (AD) is characterized by the accumulation and spread of Tau intraneuronal inclusions throughout most of the telencephalon, leaving hindbrain regions like the cerebellum and spinal cord largely spared. These neuropathological observations, along with the identification of specific vulnerable sub-populations from AD brain-derived single nuclei transcriptomics, suggest that a subset of brain regions and neuronal subtypes possess a selective vulnerability to Tau pathology. Given the inability to culture neurons from patient brains, a disease-relevant in vitro model which recapitulates these features would serve as a critical tool to validate modulators of vulnerability and resilience. Using our recently established platform for inducing endogenous Tau aggregation in human induced pluripotent stem cell (hiPSC)-derived cortical excitatory neurons via application of AD brain-derived exogenous Tau aggregates, we explored whether Tau aggregates preferentially induce aggregation in specific neuronal subtypes. We compared Tau seeding in hiPSC-derived neuron subtypes representing regional identities across the forebrain, midbrain, and hindbrain. Higher susceptibility (i.e. more Tau aggregation) was consistently observed among cortical neuron subtypes, with CTIP2-positive, somatostatin (SST)-positive cortical inhibitory neurons showing the greatest aggregation levels across hiPSC lines from multiple donors. hiPSC-neurons also delineated between the disease-specific vulnerabilities of different protein aggregates, as α-synuclein preformed fibrils showed an increased propensity to induce aggregates in midbrain dopaminergic (mDA)-like neurons, mimicking Parkinson's disease (PD)-specific susceptibility. Aggregate uptake and degradation rates were insufficient to explain differential susceptibility. The absence of a consistent transcriptional response following aggregate seeding further indicated that intrinsic neuronal subtype-specific properties could drive susceptibility. The present data provides evidence that hiPSC-neurons exhibit

[†]Ian Weidling, Gyan Srivastava, J. K. Thomas, Marie-Theres Weil are former employees of AbbVie.

*Correspondence:
Justine D. Manos
justine.manos@abbvie.com
Full list of author information is available at the end of the article

features of selective neuronal vulnerability which manifest in a cell autonomous manner, suggesting that mining intrinsic (or basal) transcriptomic signatures of more vulnerable compared to more resilient hiPSC-neurons could uncover the molecular underpinnings of differential susceptibility to protein aggregation found in a variety of neurodegenerative diseases.

Keywords hiPSC-derived neurons, Selective vulnerability, Tau, Alzheimer's disease, Parkinson's disease

Introduction

Selective vulnerability of specific neuronal populations to degeneration is a well-established feature of Alzheimer's disease (AD) [8, 26, 57]. Braak staging of AD brain tissue demonstrates selective vulnerability at a regional level, revealing a stereotypical progression of hyperphosphorylated, aggregated Tau inclusions from the locus coeruleus to the entorhinal cortex and, ultimately, throughout the cortex [6, 7, 83]. While cortical regions are highly vulnerable to AD, midbrain and hindbrain regions remain relatively free from Tau pathology during disease progression. In addition, recent studies in postmortem AD brain tissue using single nucleus RNA-sequencing (snRNA-seq) have furthered our understanding of selective vulnerability by identifying molecular signatures associated with disease progression and neuronal subclasses preferentially lost as Tau pathology increases [46, 53, 62]. One such study highlights the loss of SST-positive cortical inhibitory neurons in individuals with high AD pathology burden [54], suggesting this neuronal subtype may be particularly vulnerable to disease processes, while other studies have identified RAR-related Orphan Receptor B (RORB)-positive cortical excitatory neurons as highly susceptible to Tau tangles [45], and yet the mechanism(s) driving the susceptibility of vulnerable neurons to Tau aggregation and subsequent neuronal loss remain unknown. Modeling selective vulnerability in vitro could elucidate why certain neuronal populations develop Tau pathology and why some subtypes are more resilient.

Human induced pluripotent stem cells (hiPSCs) could represent a suitable model system for studying the underlying mechanisms of susceptibility based on their well-established capacity to differentiate to a variety of neuronal subtypes [49, 71, 77]. Indeed, a previous study differentiated hiPSCs with the familial AD (fAD) mutation APP-V717I into neurons with rostral and caudal identities, finding inherent differences in Aβ production and in responsiveness to exogenous Aβ between these neuronal subtypes [61]. Treatment with exogenous Aβ preferentially induced Tau phosphorylation in hiPSC-rostral neurons relative to hiPSC-caudal neurons, and this effect on Tau was eliminated by immunodepletion with an anti-Aβ antibody [61]. While the findings from this study support the potential utility of hiPSC-derived neuron subtypes to exhibit properties of selective vulnerability to Aβ, it remains to be determined whether hiPSC-neuron subtypes also show more direct differences in their propensity to form Tau aggregates which can progress to become neurofibrillary tangles (NFT), a pathological hallmark of AD positively correlated to cognitive decline [63]. This was recently made possible by the establishment of a Tau seeding assay in hiPSC-neurons that showed the formation of endogenous, insoluble Tau aggregates following seeding with exogenous AD brain-derived pathological Tau [51].

Here, we utilized hiPSC-derived neurons to study susceptibility to AD-relevant Tau pathology in vitro. hiPSCs were differentiated into 5 distinct neuronal populations representing neurons found in the forebrain, midbrain, or hindbrain regions. The propensity of each neuronal subtype to form endogenous Tau aggregates was examined following seeding with two separate fractions of AD–brain-derived seeding-competent Tau. Among the unique neuronal subtypes tested, CTIP2-positive, SST-positive cortical inhibitory-like hiPSC-derived neurons displayed the highest load of Tau aggregates, while hypothalamic, midbrain dopaminergic (mDA), and spinal cord-like neurons exhibited greater resilience. The ability of protein aggregates to induce susceptibility patterns consistent with human disease was not unique to aggregated Tau as α-synuclein pre-formed fibril (PFF) seeding in hiPSC-neurons showed enhanced susceptibility in midbrain dopaminergic neurons, consistent with the observed neuronal vulnerabilities in PD. Exogenous aggregate uptake and degradation rates alone could not explain the differences in the propensity of different neuron subtypes to form seeded aggregates. Furthermore, transcriptomics revealed no differences in how the neuronal subtypes responded to seeding, suggesting that baseline cell intrinsic properties may underlie the selective vulnerability of distinct hiPSC-neurons.

Materials and methods

Experimental model and subject details

Human iPSC lines

The following hiPSC lines were used in this study: SBAD3 Cl.1 (StemBANCC) RRID:CVCL_ZX55 [84], BIONi010-C (available from EBiSC www.ebisc.org; the EBiSC Bank acknowledges Bioneer A/S as the source of human

induced pluripotent stem cell line BIONi010-C-13 which was generated with support from EFPIA companies and the European Union (IMI-JU)) RRID:CVCL_1E68, ACS-1023 (ATCC) RRID:CVCL_A324, and BIOMEDi004-A (BioMedX) RRID:CVCL_UL83 [73] and a subclone derived from IPSC0028/SIGi001-A (Sigma-Aldrich) RRID:CVCL_EE38. Detailed hiPSC donor line information can be found in Table 1. Characterization of the hiPSC lines confirming expression of markers of the undifferentiated state and a normal karyotype were performed by the manufacturers. Human iPSC maintenance was performed as described previously [51].

Brain tissue for isolation of SI-AD material

Frozen human frontal cortical brain tissue from AD (Braak stage V/VI) and non-AD (Braak stage 0/I) male and female donors used in preparing sarkosyl-insoluble Tau aggregates were generously provided by the Massachusetts Alzheimer's Disease Research Center or purchased from Folio (now Discovery Life Sciences) and Banner Health.

Brain tissue for isolation of SS-AD material

Anonymized human brain samples were obtained from The Netherlands Brain Bank (NBB), Netherlands Institute for Neuroscience, Amsterdam (open access: www.brainbank.nl). All material has been collected from donors for whom a written informed consent for a brain autopsy and the use of the material and clinical information for research purposes had been obtained by the NBB.

hiPSC differentiation to distinct neuronal subtypes

Neural induction from hiPSCs to NPCs was performed in a single batch per subtype per donor line.

Cortical inhibitory hiPSC-neurons

Pluripotent hiPSCs were differentiated to ventral forebrain neural progenitors and subsequently underwent terminal differentiation to cortical inhibitory hiPSC-neurons according to a modified published protocol [12]. Differentiation was initiated as described previously [51]. On day 0 (beginning of hiPSC neural induction), confluent hiPSCs were switched to Essential 6 media (Thermo Fisher) supplemented with 500 nM LDN193189 (StemGent) and 10 µM SB431542 (R&D Systems). Neural induction was carried out from day 0 to day 17 as described previously with slight modifications [51]. On day 17, hiPSC-derived neural progenitor cells (hiPSC-NPCs) were collected with Accutase, resuspended in N2B27 medium (Advanced DMEM/F12, Neurobasal medium, N2 supplement, B27 supplement without vitamin A, pen/strep, GlutaMax; Thermo Fisher) +10% DMSO at 10 million cells per mL, and frozen overnight at −80°C in a controlled vessel at 1 °C per minute before being transferred to LN_2 vapor for long-term storage. Synchronization of hiPSC-NPC differentiation to cortical inhibitory neurons is achieved by thawing frozen vials (considered "DIV-8") onto 77.5 µg/mL Matrigel®-coated (Growth Factor Reduced; Corning) plates at 350,000 cells per cm^2 in N2B27 medium supplemented with 10 µM Y-27632 (Millipore) and subsequent culturing with N2B27 medium. Neuronal differentiation was promoted with the addition of the γ-secretase inhibitor RO4929097 (VWR) at 500 nM on DIV-5. On DIV0 (final hiPSC-neuron replating), cells were plated as described previously [51]. In rare cases where an hiPSC line showed evidence of a dorsal identity following this protocol, differentiation was repeated with smoothened agonist (SAG) to activate hedgehog signaling and encourage ventralization.

Hypothalamic hiPSC-neurons

Pluripotent hiPSCs were differentiated to ventral forebrain neural progenitors as described above. Ventral forebrain hiPSC-NPCs were thawed and plated on DIV-8 as described previously [51] and subsequently cultured with N2B27 medium supplemented with 500 nM SAG (Sigma), 100 ng/mL recombinant FGF8-A (StemCell Technologies), and 10 ng/mL recombinant GDF-2 (BMP-9) (Peprotech) until DIV0. Neuronal differentiation was promoted with the addition of the γ-secretase inhibitor RO4929097 (VWR) at 500 nM on DIV-5. On DIV0,

Table 1 Human iPSC donor line information

Line	Source	Donor Age/Sex/Ethnicity	Donor tissue	Reprogramming method	Reprogramming factors	APOE
IPSC0028	Sigma/Janssen	24/F/Caucasian	Epithelial cells	Retrovirus	OSKM	3/4
BIONi010-C	EBiSC	19/M/African American	Dermal fibroblasts	Episomal	OSKML + shp53	3/4
SBAD3	StemBANCC	31/F/Unknown	Fibroblasts	Sendai	OSKM	2/3
ACS-1023	ATCC	36/F/Caucasian	Fibroblasts	Retrovirus	OSKM	3/3
BIOMEDi004-A	BioMedX	64/M/Caucasian	Fibroblasts	ReproRNA	OKSGM	3/3

cells were plated as described previously [51], except at ~190,000 cells per cm^2 (60,000 cells per 96-well).

Cortical excitatory hiPSC-neurons

Pluripotent hiPSCs were differentiated to dorsal forebrain neural progenitors and subsequently underwent terminal differentiation to cortical excitatory hiPSC-neurons as described previously [51]. In cases with evidence of high neural crest contamination (indicates high Wnt signaling at pluripotent stage), differentiation was repeated without CHIR99021.

mDA hiPSC-neurons

Pluripotent hiPSCs were differentiated to midbrain floorplate NPCs and subsequent differentiation to midbrain dopaminergic hiPSC-neurons according to a modified published protocol [74]. Differentiation was initiated using hiPSC cultures containing large homogeneous colonies with phase bright borders and low levels of spontaneous differentiation. Cells were harvested with Accutase and plated at a density specific to each hiPSC donor line onto 77.5 µg/mL Matrigel-coated 10 cm dishes (Day −1) in StemFlex Complete supplemented with 10 µM Y-27632. When hiPSC cultures reached ~75% confluency (typically Day 2), cells were harvested with ReLeSR (StemCell Technologies) and plated onto uncoated 10 cm dishes in N2B27 medium (Advanced DMEM/F12, Neurobasal medium, N2 supplement, B27 supplement without vitamin A, pen/strep, GlutaMax; ThermoFisher) supplemented with 10 µM SB431542 (R&D systems), 50 nM LDN193189 (StemGent), 0.75 µM CHIR99021 (R&D Systems), 0.5 µM SAG (Sigma), 200 µM Ascorbic Acid (Sigma), and 5 µM Y-27632 (Millipore) to allow for embryoid body formation. Embryoid bodies were subsequently fed N2B27 medium (Advanced DMEM/F12, Neurobasal medium, N2 supplement, B27 supplement without vitamin A, pen/strep, GlutaMax; ThermoFisher) supplemented with 10 µM SB431542 (R&D systems), 50 nM LDN193189 (StemGent), 0.75 µM CHIR99021 (R&D Systems), 0.5 µM SAG (Sigma), 200 µM Ascorbic Acid (Sigma) every other day until day 8, at which time they were dissociated via trituration and plated at a density specific to each hiPSC donor line onto 77.5 µg/mL Matrigel-coated 12-well plates. On day 9, cells were fed N2B27 medium (Advanced DMEM/F12, Neurobasal medium, N2 supplement, B27 supplement without vitamin A, pen/strep, GlutaMax; ThermoFisher) supplemented with 10 µM SB431542 (R&D systems), 50 nM LDN193189 (StemGent), 0.75 µM CHIR99021 (R&D Systems), 0.5 µM SAG (Sigma), and 200 µM Ascorbic Acid (Sigma). On day 10, cells were fed N2B27 medium (Advanced DMEM/F12, Neurobasal medium, N2 supplement, B27 supplement without vitamin A, pen/strep, GlutaMax; ThermoFisher) supplemented with 2.5 µM SB431542 (R&D systems), 50 nM LDN193189 (StemGent), 0.75 µM CHIR99021 (R&D Systems), 0.5 µM SAG (Sigma), and 200 µM Ascorbic Acid (Sigma). On day 12, cells were harvested with Accutase and plated at a density of 1.25 million cells per well onto 77.5 µg/mL Matrigel-coated 6-well plates in N2B27 medium (Advanced DMEM/F12, Neurobasal medium, N2 supplement, B27 supplement without vitamin A, pen/strep, GlutaMax; ThermoFisher) supplemented with 2.5 µM SB431542 (R&D systems), 50 nM LDN193189 (StemGent), 0.75 µM CHIR99021 (R&D Systems), 0.5 µM SAG (Sigma), 200 µM Ascorbic Acid (Sigma), and 5 µM Y-27632 (Millipore). Following this replating step, cells were cultured and replated two more times following the same procedure at a density of 850,000 cells per well in 77.5 µg/mL Matrigel-coated 6-well plates. hiPSC-NPCs were subsequently frozen as described previously [51]. Synchronization of hiPSC-NPC differentiation to neurons was achieved by thawing frozen vials (considered "DIV −15") onto 77.5 µg/mL Matrigel-coated plates at 350,000 cells per cm^2 in N2B27 medium supplemented with 3 µM CHIR99021 (R&D Systems), 0.5 µM SAG (Sigma), 200 µM Ascorbic Acid (Sigma), and 10 µM Y-27632 (Millipore). The following day (DIV-14), cells were fed with N2B27 medium supplemented with 3 µM CHIR99021 (R&D Systems), 0.5 µM SAG (Sigma), and 200 µM Ascorbic Acid before subsequent culturing in N2B27 medium supplemented with 0.7 µM CHIR99021 (R&D Systems), 0.5 µM SAG (Sigma), and 200 µM Ascorbic Acid (Sigma). On DIV-9, hiPSC-NPCs were harvested with Accutase and plated onto 77.5 µg/mL Matrigel-coated plates at a density of 2 million cells per well in N2B27 medium supplemented with 0.7 µM CHIR99021 (R&D Systems), 0.5 µM SAG (Sigma), 200 µM Ascorbic Acid (Sigma), and 10 µM Y-27632 (Millipore). Cells were subsequently cultured in N2B27 medium supplemented with 10 ng/mL BDNF, 10 ng/mL GDNF, 500 µM dcAMP, 1 ng/mL TGFβ3 (R&D Systems), 2.5 ng/mL Activin A, 200 µM Ascorbic Acid (Sigma), and 10 µM DAPT (Cayman Chemical). Neuronal differentiation was encouraged with the addition of the γ-secretase inhibitor RO4929097 (VWR) at 500 nM on DIV-5. For final neuron replating, black 96-well plates (Corning/Fisher 353,219 or PerkinElmer Cell Carrier Ultra) were treated with 0.01% Poly-L-ornithine (PLO; Sigma) solution overnight at room temperature. The next day, PLO was completely aspirated and plates were then coated with 28 µg/mL Matrigel diluted in DMEM/F12 + HEPES and stored at 4 °C overnight. On DIV 0, cells were harvested with Accutase, passed through a 40 µm cell strainer (VWR) to remove residual cell clusters, centrifuged at 300 ×g for 5 min, and plated into PLO-treated/Matrigel-coated

plates at ~110,000 cells per cm^2 (35,000 cells per 96-well) in NB27 + medium (Neurobasal Plus medium, B27 Plus supplement, pen/strep, GlutaMax; ThermoFisher) supplemented with 10 µM Y-27632, 500 nM RO4929097, 10 ng/mL BDNF, 200 µM Ascorbic Acid, 250 µM dcAMP, 5 ng/mL GDNF, and 1 µg/mL Laminin. On DIV 2, hiPSC-neurons were treated with 0.5 µg/mL Mitomycin-C (Sigma) diluted in Neuronal Maintenance Medium (NMM; NB27 + supplemented with 10 ng/mL BDNF, 200 µM Ascorbic Acid, 250 µM dcAMP, 5 ng/mL GDNF, and 1 µg/mL Laminin) for 1 h in the incubator (37 °C with 5% CO_2). After incubation, two-thirds of the well volume was removed and replaced with fresh NMM supplemented with 500 nM RO4929097. The hiPSC-neurons were maintained with half volume media changes twice weekly with fresh NMM.

Spinal cord hiPSC-neurons

Pluripotent hiPSCs were differentiated to spinal cord NPCs according to a modified published protocol [21]. Differentiation was initiated as described previously [51]. On day 0 (beginning of hiPSC neural induction), confluent hiPSCs were switched to N2B27 medium (Advanced DMEM/F12, Neurobasal medium, N2 supplement, B27 supplement without vitamin A, pen/strep, GlutaMax; Thermo Fisher) supplemented with 500 nM LDN193189 (StemGent), 10 µM SB431542 (R&D Systems), and 1 µM CHIR99021 (R&D Systems). Starting day 3, Laminin (Sigma) was added at 1 µg/mL concentration to help prevent cell lifting. Six days after initiation, the cells were harvested with Accutase and plated at 1.5 million cells per cm^2 in N2B27 medium supplemented with 500 nM LDN193189 (StemGent), 10 µM SB431542 (R&D Systems), 1 µM CHIR99021 (R&D Systems), 100 nM retinoic acid (R&D Systems), 500 nM SAG (Sigma), and 10 µM Y-27632 (Millipore). 10 ng/mL FGF2 (Millipore) was briefly added to the medium until day 13. On day 13, hiPSC-NPCs were collected with Accutase, resuspended in N2B27 medium + 10% DMSO at 10 million cells per mL, and frozen overnight at − 80 °C in a controlled vessel at 1 °C per minute before being transferred to LN_2 vapor for long-term storage. In cases with evidence of high neural crest contamination (indicates high Wnt signaling at pluripotent stage), differentiation was repeated without CHIR99021 after day 6. Synchronization of hiPSC-NPC differentiation to spinal cord neurons is achieved by thawing frozen vials (considered "DIV-8") onto 77.5 µg/mL Matrigel®-coated (Growth Factor Reduced; Corning) plates at 350,000 cells per cm^2 in N2B27 medium supplemented with 10 µM Y-27632 (Millipore) and subsequent culturing with N2B27 medium supplemented with 500 nM retinoic acid (R&D Systems) and 100 nM SAG (Sigma). Neuronal differentiation was encouraged with the addition of the γ-secretase inhibitor RO4929097 (VWR) at 500 nM on DIV-5. On DIV0 (final hiPSC-neuron replating), cells were plated as described previously [51], except at ~190,000 cells per cm2 (60,000 cells per 96-well).

RNA Isolation and quantitative PCR

Total RNA was prepared from hiPSC cultures using the MagMAX™ mirVana™ Total RNA Isolation Kit (Thermo Fisher) according to the manufacturer's instructions. The integrity (RIN score) and concentration of the RNA was determined using an Agilent TapeStation. Reverse transcription was performed with Superscript IV VILO (Thermo Fisher) in a 20 µl reaction with 16 µl per sample. The cDNA yield for each reaction was determined using Quant-iT™ OliGreen® reagent (Thermo Fisher). Samples were subjected to qPCR analysis using the Juno/Biomark HD high throughput platform (Fluidigm). Briefly, cDNA was preamplified for 15 PCR cycles in a multiplex fashion using a panel of 96 Taqman assays (Thermo Fisher; Table 2). Following tenfold dilution with water, the preamplified samples were prepared for loading onto the integrated fluidic circuit in accordance with the manufacturer's protocol. Data analysis was performed using the GenEx Professional software package, version 6 (MultiD Analyses AB). Starting with the raw Ct values, the Normfinder feature of the software was used to identify the most robust normalization scheme, resulting in the use of the 12 most stable transcripts to convert raw Cts into delta Ct values (referred to as global normalization).

Western blots

Preparation of cell lysates

DIV16 hiPSC-neurons were rinsed with ice-cold PBS and MPER lysis buffer supplemented with cOmplete™ protease inhibitors (Millipore) and PhosSTOP™ (Millipore) was added directly to adherent cells. Cells were incubated in lysis buffer for 5 min on ice. Cell lysates were then transferred to microcentrifuge tubes and spun at 3,000 ×g for 5 min. The supernatant was collected and technical and biological replicates for each hiPSC-neuron subtype were pooled. Total protein quantification was performed using the Micro-BCA™ Protein assay (Thermo Fisher). Cell lysates were normalized by total protein concentration and LDS sample buffer (Thermo Fisher) and reducing agent containing DTT (Thermo Fisher) were added.

Blotting

Cell lysates were boiled at 95 °C for 5 min on a heat block and then separated by gel electrophoresis on a 4–12% NuPAGE Bis–Tris gel (Thermo Fisher). Precision Plus Protein Dual Color Standard (Bio-Rad) was

Table 2 Gene targets for fluidigm qPCR neuronal characterization panel

Gene name	Gene category	assay ID
ADARB2	Inhibitory neuron	Hs00218878_m1
ALDH1A2	Dentate gyrus neuron	Hs00180254_m1
AQP4	Astrocyte	Hs00242342_m1
ASCL1	Immature neuron	Hs00269932_m1
B3GAT2	CA3 neuron	Hs00369834_m1
BCL11B	Cortical neuron	Hs01102259_m1
C1QL2	Dentate gyrus neuron	Hs00704398_s1
CADPS2	Dentate gyrus neuron	Hs00604528_m1
CALB1	Interneuron	Hs01077197_m1
CALB2	Interneuron	Hs00242372_m1
CAMK2A	Excitatory neuron	Hs00947041_m1
CCDC85A	CA3 neuron	Hs00287585_m1
CCK	Interneuron	Hs00174937_m1
CHAT	Cholinergic neuron	Hs00758143_m1
CUX1	Cortical neuron	Hs00738851_m1
DBH	Noradrenergic neuron	Hs01089840_m1
DCX	Pan-neuronal	Hs00167057_m1
DDC	Dopaminergic neuron	Hs01105048_m1
DOCK10	CA1 neuron	Hs00391515_m1
EIF4A2	Housekeeping	Hs00756996_g1
ELAVL2	CA3 neuron	Hs00270011_m1
EN1	Midbrain neuron	Hs00154977_m1
FEZF2	Cortical neuron	Hs01115572_g1
FOXA2	Midbrain neuron	Hs00232764_m1
FOXG1	Forebrain neuron	Hs01850784_s1
FOXP2	Cortical neuron	Hs00362818_m1
GAD1	Inhibitory neuron	Hs01065893_m1
GAPDH	Housekeeping	Hs02786624_g1
GRIK4	CA3 neuron	Hs00205979_m1
HOXC5	Hindbrain neuron	Hs00232747_m1
IGSF3	CA3 neuron	Hs01035583_m1
ISL1	Peripheral neuron	Hs00158126_m1
LAMP5	Cortical neuron	Hs00202136_m1
LEF1	Wnt signaling	Hs01547250_m1
LHX2	Hippocampal neuron	Hs00180351_m1
LHX6	Interneuron	Hs00232660_m1
LHX9	Hippocampal neuron	Hs00294879_m1
LMX1A	Dopaminergic neuron	Hs00898455_m1
MAP2	Pan-neuronal	Hs00258900_m1
MAPT_2192(3R/4R)	Pan-neuronal	Hs00902192_m1
MAPT_2312(4R)	Mature neuron	Hs00902312_m1
MNX1	Motor neuron	Hs00907365_m1
MSH6	Broadly expressed	Hs00943000_m1
NANOG	Pluripotency marker	Hs02387400_g1
NECAB1	Cortical neuron	Hs00332733_m1
NEUROD1	Cortical neuron	Hs01922995_s1
NGFR	Neural crest	Hs00609976_m1
NKX2-1	Neural progenitor	Hs00968940_m1
NKX6-1	Neural progenitor	Hs00222355_m1
NR4 A2	Dopaminergic neuron	Hs01117527_g1
NTNG1	Excitatory neuron	Hs01552822_m1
NTRK1	Sensory neuron	Hs01021011_m1
NTRK2	Sensory neuron	Hs00178811_m1
OLIG2	Oligodendrocyte/motor neuron	Hs00300164_s1
OTX2	VTA dopaminergic neuron	Hs00222238_m1
PAX3	Peripheral neuron	Hs00249950_m1
PAX6	Dorsal forebrain	Hs01088114_m1
PCBD1	Broadly expressed	Hs01548084_g1
PDGFRA	Oligodendrocyte	Hs00998018_m1
PDYN	Dentate gyrus neuron	Hs00225770_m1
PHOX2A	Dorsal hindbrain progenitor	Hs00605931_mh
PHOX2B	Dorsal hindbrain progenitor	Hs00243679_m1
PITX3	Dopaminergic neuron	Hs01013935_g1
POU3F1	CA3 neuron	Hs00538614_s1
POU3F2	Cortical neuron	Hs00271595_s1
POU5F1	Pluripotency marker	Hs04260367_gh
PPP1R1B	Neuron enriched	Hs00259967_m1
PRKCD	Dentate gyrus neuron	Hs01099047_m1
PROX1	Dentate gyrus neuron	Hs00896293_m1
PVALB	Interneuron	Hs00161045_m1
QDPR	Brain enriched	Hs01077088_m1
RBFOX3	Pan-neuronal	Hs01370654_m1
RELN	Cortical neuron	Hs01022646_m1
RORB	Cortical neuron	Hs00199445_m1
RPL13	Housekeeping	Hs00744303_s1
SAMD3	Dentate gyrus neuron	Hs00381007_m1
SATB2	Cortical neuron	Hs01546836_s1
SCGN	CA3 neuron	Hs00199630_m1
SLC17A6	Excitatory neuron	Hs00220439_m1
SLC17A7	Excitatory neuron	Hs00220404_m1
SLC18A3	Cholinergic neuron	Hs00268179_s1
SLC1A3	Astrocyte	Hs00904823_g1
SLC32A1	Inhibitory neuron	Hs00369773_m1
SLC6A3	Dopaminergic neuron	Hs00997374_m1
SOX1	Neural progenitor	Hs01057642_s1
SST	Interneuron	Hs00356144_m1
SYN1	Pan-neuronal	Hs00199577_m1
SYP	Pan-neuronal	Hs00300531_m1
TBR1	Cortical neuron	Hs00232429_m1
TFAP2A	Non-neural ectoderm	Hs01029413_m1
TH	Dopaminergic neuron	Hs00165941_m1
THEMIS	Cortical neuron	Hs01041269_m1
TSPAN18	CA3 neuron	Hs00901276_m1
TSPAN7	Hippocampal neuron	Hs00190284_m1
TUBB3	Pan-neuronal	Hs00801390_s1
VIP	Interneuron	Hs00175021_m1

included on each gel to assist with molecular weight estimation. The gel was transferred using the iBlot2 dry blotting system (Thermo Fisher) onto a pre-activated PVDF membrane using the P0 program. Membranes were blocked using Intercept© (PBS) blocking buffer (LI-COR Biosciences) for 1 h at RT on a shaker prior to primary antibody addition. Membranes were incubated with primary antibodies (Table 3) overnight on a shaker at 4 °C. The following day, membranes were washed with PBST, then incubated with Licor IRDye™ anti-rabbit (680RD) and anti-mouse (800 CW) secondary antibodies (LI-COR Biosciences) at 1:5000 for 1 h at RT. The membranes were then washed with PBST and imaged on the Licor Odyssey CLX system (LI-COR Biosciences) RRID:SCR_014579.

Single cell RNA-seq

Sample collection

DIV14 hiPSC-neurons were harvested with Accutase (Thermo Fisher) and resuspended at a concentration of 200 cells/µL in 0.4% BSA/PBS. 43.1 µL of cell suspension (~ 8,600 cells) was input for single cell library generation.

Library generation and sequencing

Single-cell RNA-seq libraries were prepared from each sample using the Chromium Single Cell 3′ Reagent kit (10X Genomics) following manufacturer's instructions. Briefly, nanoliter-scale Gel Beads -in-emulsion (GEMs) were generated by combining barcoded Single Cell 3′ v3.1 Gel Beads (10X Genomics), a master mix containing cells and partition oil onto Chromium

Table 3 List of primary antibodies

Antibody	Source	Catalogue #	Host	RRID
HT7	Thermo Fisher	MN1000	Mouse IgG1 monoclonal	AB_2314654
MAP2	Abcam	ab5392	Chicken polyclonal IgY	AB_2138153
CTIP2	Abcam	ab18465	Rat monoclonal IgG2a; 25B6	AB_2064130
TBR1	Abcam	ab183032	Rabbit monoclonal	AB_2936859
FOXG1	Abcam	ab18259	Rabbit polyclonal	AB_732415
FOXA2	Abcam	ab108422	Rabbit monoclonal	AB_11157157
HOXB4	Abcam	ab76093	Rabbit monoclonal	AB_2119271
Tyrosine Hydroxylase	Pel-Freez	P40101-150	Rabbit polyclonal	AB_2617184
β-actin	Sigma-Aldrich	A1978	Mouse monoclonal	AB_476692
TauC	Dako (Agilent)	A0024	Rabbit polyclonal	AB_10013724
MC1(conformational tau)	AbbVie	MC1	Mouse monoclonal IgG1	Produced internally by AbbVie
HJ9.2 (epitope: amino acids 4–8 of Tau)	AbbVie	HJ9.2	Mouse IgG2b	Produced internally by AbbVie
PHF1 (Tau pSer396/pS404)	P. Davies Albert Einstein College of Medicine; New York; USA	PHF1	Mouse monoclonal IgG1	AB_2315150
MC1 (conformational tau)	P. Davies Albert Einstein College of Medicine; New York; USA	MC1	Mouse IgG1	AB_2314773
Tau12 (anti-Tau, 6–18)	BioLegend	806,502	Mouse monoclonal	AB_2564708
HT7 – Biotinylated	Thermo Fisher	MN1000B	Mouse monoclonal	AB_223453
AT100 (Tau pThr212/pSer214)	Thermo Fisher	MN1060	Mouse monoclonal	AB_223652
AT180 (Tau pThr231)	Thermo Fisher	MN1040	Mouse monoclonal	AB_223649
Nanog	R&D	AF1997	Goat polyclonal	AB_355097
Oct4	R&D	AF1759	Goat polyclonal	AB_354975
PAX6	Biolegend	901,301	Rabbit polyclonal	AB_2565003
AP2α	DSHB	5e4	Mouse monoclonal IgG1	AB_528085
SOX10	R&D	AF2864	Goat polyclonal	AB_442208
OTX2	R&D	AF1979	Goat polyclonal	AB_2157172
OLIG2	Millipore	AB9610	Rabbit polyclonal	AB_570666
NKX6.1	DSHB	F55 A10	Mouse monoclonal IgG1	AB_532378
pSynuclein Ser129 (D1R1R)	CST	23,706	Rabbit monoclonal	AB_2798868
LMX1A	Abcam	ab139726	Rabbit polyclonal	AB_2827684
TUBB3 (TUJ1)	BioLegend	801,201	Mouse monoclonal IgG2a	AB_2313773

Next GEM Chip G (10X Genomics). Reverse transcription of GEM was performed to produce barcoded, full-length cDNA from poly-adenylated mRNA. Following the GEM incubation, GEM cleanup was performed using silane magnetic beads to obtain purified first-strand cDNA. Barcoded, full-length cDNA was then amplified via PCR and 25% of generated cDNA was used for library construction. Quality control of cDNA and prepared libraries was performed using the high sensitivity D5000 ScreenTape assay on a 4200 TapeStation System (Agilent) RRID:SCR_018435. Libraries were sequenced using a NovaSeq 6000 S4 200 cycle flow cell (Illumina) RRID:SCR_016387.

Data analysis

Sequence alignment and pre-processing of data was conducted using 10 ×Cell Ranger 7.0 software RRID:SCR_023221. The count matrix was then analyzed using Seurat 4.3.0 [33, 70, 75] RRID:SCR_007322. While creating a Seurat object, standard filtering options (min.cells =3; min.features =200) were applied. scDblFinder [29] RRID:SCR_022700 was used for doublet identification. The intronic ratio was identified and cells with an intronic ratio greater than 50% were removed. The median absolute deviation (MAD) cut-off was used to remove low-quality or outlier cells from the datasets. Cells containing greater than 15% mitochondrial genes and cells containing less than 2000 features were removed. Data was normalized using the global-scaling normalization method after removing unwanted cells from the dataset. 3000 highly variable genes were used for downstream analysis. Principal component analysis was performed to reduce dimensionality and 20 principal components were used to identify clusters. Neuron maturity index was applied as described previously [36].

Bulk RNA-seq

Sample treatment and RNA extraction

DIV16 hiPSC-neurons were seeded with 0.5 nM SI-AD or treated with an equal volume of either SI-Control material or PBS. 72 h following treatment, RNA lysates were collected in MagMAX™ lysis buffer (Thermo Fisher). Total RNA was prepared from hiPSC cultures using the MagMAX™ mirVana™ Total RNA Isolation Kit (Thermo Fisher) as described above.

Library preparation with PolyA SELECTION and illumina sequencing

RNA library preparation, and sequencing were conducted at Azenta Life Sciences (South Plainfield, NJ, USA) as follows:

RNA samples were quantified using Qubit 2.0 Fluorometer (Life Technologies) RRID:SCR_020553 and RNA integrity was checked using Agilent TapeStation 4200 (Agilent) RRID:SCR_018435.

Strand-specific RNA sequencing libraries were prepared using the NEBNext Ultra II Directional RNA Library Prep Kit for Illumina following manufacturer's instructions (NEB, Ipswich, MA, USA). Briefly, mRNAs were enriched with oligo(dT) beads and then fragmented for 8 min at 94 °C. cDNA were subsequently synthesized. During second strand synthesis, the DNA was marked by incorporating dUTP. cDNA fragments were then adenylated at 3'ends, and index adapters were ligated to cDNA fragments. Limited cycle PCR was used for library enrichment. The incorporated dUTP in the second strand cDNA quenched the amplification of the second strand, which preserves the strand specificity. The sequencing library was validated on the Agilent TapeStation (Agilent) RRID:SCR_018435, and quantified by using Qubit 2.0 Fluorometer (Thermo Fisher) RRID:SCR_020553 as well as by quantitative PCR (KAPA Biosystems).

The sequencing libraries were clustered on the flowcell and subsequently loaded on an Illumina sequencer RRID:SCR_016387 according to manufacturer's instructions. The samples were sequenced using a 2 ×150bp paired end (PE) configuration. Image analysis and base calling were conducted by the control software. Raw sequence data (.bcl files) generated by the sequencer were converted into fastq files and de-multiplexed using Illumina's bcl2fastq 2.20 software RRID:SCR_015058. One mismatch was allowed for index sequence identification.

Data analysis

Paired-end RNA-seq reads were trimmed using TRIMGalore RRID:SCR_011847, which used Cutadapt version 2.10 [52] RRID:SCR_011841. The reads were aligned to hg38 using STAR [20, 47] RRID:SCR_004463 and gene-level counts were generated using featureCounts [47] (non-default parameters specified: –primary, –ignoreDup) RRID:SCR_012919. Limma-voom was used for differential expression analysis RRID:SCR_010943. Genes with CPM >2 in > = 6 samples were tested for differential expression. A threshold of adj.P.Val <0.05 was used to determine differentially expression/significance. For Gene Ontology [1, 2] enrichment analyses, hypergeometric tests were performed using clusterProfiler [88, 90] RRID:SCR_016884. Background gene lists included all genes tested for differential expression.

Cell characterization immunofluorescence

PFA fixation

hiPSCs, hiPSC-NPCs and hiPSC-neurons were fixed by a 15 min incubation at room temperature in 3% paraformaldehyde solution in PBS (Thermo Fisher), followed by

three PBS washes. Fixed cells were subsequently stored in DPBS with calcium/magnesium (Thermo Fisher) at 4 °C.

Immunofluorescence staining

Prior to incubation with primary antibody, cells were incubated for 1 h in blocking buffer composed of 3% Bovine Serum Albumin (BSA) (Millipore) and 0.3% Triton X-100 (Sigma) in PBS. Following blocking, cells were incubated with primary antibodies (Table 3), diluted to the appropriate concentration in blocking buffer and filtered through a 0.22 µm Spin-X column (Corning), overnight at 4 °C, with shaking. The following day, primary antibody solution was removed and cells were washed three times with PBS. Cells were then incubated with Alexa Fluor™ secondary antibody (Thermo Fisher), diluted 1:500 in blocking buffer and filtered through a 0.22 µm Spin-X column (Corning), for 1 h at room temperature, with shaking. Following incubation with secondary antibody, cells were incubated with Hoechst 33,342 solution (Invitrogen), diluted 1:5000 in PBS, for 15 min at room temperature, with shaking. Cells were then washed two times with PBS and imaged immediately on an Operetta CLS high content imaging system (PerkinElmer) RRID:SCR_018810 or stored at 4 °C, protected from light, for subsequent imaging. Images are displayed with consistent settings across donor lines or cell types for comparison. Quantification of DIV21 hiPSC-neuron % Nuclei, HT7 (Tau) area, MAP2 area, and TH intensity were performed using Harmony software (PerkinElmer) RRID:SCR_018809.

Brain-derived Tau aggregates

Sarkosyl-insoluble protein preparation and characterization (SI-AD)

Frozen tissue was handled as described previously [51]. Briefly, we first divided large (usually > 10 g/piece) frozen tissues into smaller pieces (0.5–1 mg/piece) for randomization, then prepared aliquots of large stocks of lysates made from multiple pieces of tissue for future use. Tau pathology of these tissues was confirmed using the HTRF Tau aggregation assay (Cisbio) and HEK biosensor seeding. Importantly, lysates derived from AD brains that have low levels of Tau aggregates were excluded from further use (data not shown). Sarkosyl-insoluble protein (SI-AD and SI-Control) were prepared and characterized as described previously [51] from pathology-confirmed AD or non-AD donors purchased from Folio (now Discovery Life Sciences) and Banner Health brain bank.

Sarkosyl-soluble protein preparation and characterization (SS-AD)

Frozen samples from frontal and temporal cortex of 15 individual AD patients with Braak stages V-VI were homogenized, pooled and the TBS-soluble fraction S1 as well as the corresponding sarkosyl-insoluble pellet was generated from the pool as described previously [72]. To purify soluble seeding competent species, the TBS-soluble S1 fraction was adjusted to 1% N-lauroyl-sarkosine (Sigma) and incubated for 1.5 h at room temperature, followed by a high-speed centrifugation at 150 000 ×g for 3 h at 4 °C, yielding the sarkosyl-soluble supernatant (SS1) fraction. Ultracentrifugation columns (Vivaspin 30 K concentrator spin columns; Sartorius) were used according to manufacturer's instructions to exchange the buffer to PBS and achieve app. sixfold concentration of the SS1 fraction. Further de-salting of the concentrate was achieved with 7 K ZebaSpin desalting columns (Thermo Fisher), and the volume of the de-salted sample was adjusted back to its original concentration by app. sixfold dilution in PBS +0.1% Pluriol (Pluronic F68). For immunoprecipitation, antibodies HJ9.2 (epitope: amino acids 4–8 of Tau, mouse IgG2b) and PHF1 (Tau pSer396/404, mouse IgG1; kindly provided by Peter Davies to AbbVie through a Material Transfer Agreement with Feinstein Institute) RRID:AB_2315150 were bound and cross-linked to magnetic anti-mouse Dynabeads (Thermo Fisher using dimethylpimelimidate (DMP, Thermo Fisher) in 0.2 M triethanolamine/HCl pH 8.2 according to manufacturer's instructions. Beads linked to HJ9.2 and PHF1 were mixed at a 1:1 ratio, washed with PBS +0.1% Pluriol and added to the de-salted SS1 fraction. After 20 h incubation at 6 °C on a rocking platform, beads were washed with PBS +0.1% Pluriol and subjected to an elution with competition peptides spanning the respective antibody epitope (PHF1 competition peptide: H-Arg-Glu-Asn-Ala-Lys-Ala-Lys-Thr-Asp-His-Gly-Ala-Glu-Ile-Val-Tyr-Lys-Ser(PO_3H_2)-Pro-Val-Val-Ser-Gly-Asp-Thr-Ser(PO_3H_2)-Pro-Arg-His-Leu-OH;

HJ9.2 competition peptide: H-Glu-Pro-Arg-Gln-Glu-Phe-Glu-Val-Met-Glu-Asp-His-Ala-Gly-Thr-Tyr-Gly-Leu-Gly-OH). Peptides were dissolved at 1.2 mg/ml each in PBS +0.1% Pluriol, mixed at a 1:1 ratio and cleared by a 15 min centrifugation at 16 200 ×g, followed by filtration through a 30 kDa cutoff filter column (Vivaspin, GE Healthcare). Immunoprecipitation beads were exposed to the peptide solution for 90 min at 37 °C with shaking, and the supernatant was collected. After a second, 30 min incubation at 37 °C of the beads with fresh competition peptide solution, the two eluate fractions were combined (= peptide elution). The competition peptides were removed from these eluate fractions using ultracentrifugation columns (Vivaspin concentrator spin columns; Sartorius, 30 kDa cutoff). The beads were subsequently exposed to two additional elution steps using a low pH elution buffer (100 mM glycine/HCl, pH 2.8 +140 mM NaCl +0.1% Pluriol) for 2 min at room temperature. Low

pH eluates were neutralized using 2 M Tris HCl pH 8.5 (1:40 dilution) for subsequent SDS-PAGE analysis. All fractions were shock frozen on dry ice and stored at −80 °C until further use.

ELISA- based profiling of HJ9.2 and PHF1 antibody binding properties

For ELISA analysis, recombinant human 2N4R Tau protein was generated and subjected to heparin-based aggregation to generate recombinant PHFs as described [51]. Both recombinant Tau fibrils and sarkosyl-insoluble AD brain fractions (SI-AD) were either used in their native state or after a denaturation treatment consisting of the addition of an equal volume of 2× Laemmli buffer (Bio-Rad) supplemented with 100 mM DTT and 5 min heat treatment at 98 °C.

For absolute quantification of total Tau and phospho-Tau, recombinant human 2N4R Tau produced in E. coli or in Sf9 insect cells, respectively, were used as a standard [3]. Colorimetric sandwich ELISAs using HJ9.2 and PHF1 as capture and biotinylated Tau12 RRID:AB_2564708 as detection antibodies were used, for quantification of total Tau, Tau12 was used as a capture and biotinylated HT7 antibody RRID:AB_223453 as a detection reagent. ELISA procedures are described in detail elsewhere [4]. For the determination of binding profiles to native and denatured antigens, dilution series were prepared for all antigens and ELISA-based dose–response curves were generated for each antibody. GraphPad Prism software was used for curve fitting and calculation of the area under the curve (AUC) values for each antibody/antigen combination to enable a comparison of the antibody binding profiles.

SDS-PAGE analysis of SS-AD protein

Eluates as well as final SS-AD preparations were run on 4–20% Criterion TGX SDS-PAGE gels in parallel with recombinant human 2N4R Tau as a standard. Silver staining was performed according to Blum et al., 1987 [5]: Gels were fixed with a mix of 50% ethanol and 12% acetic acid in H_2O overnight, followed by a 1 h wash in 50% ethanol and 12% acetic acid in H_2O. Three 20 min washes with 50% ethanol in H_2O were performed, followed by a 1 min sensitization step using 0.2 g $Na_2S_2O_3$ in 500 ml H_2O. Gels were washed three times for 20 s in H_2O and stained for 20 min with 0.4 g $AgNO_3$ in 200 ml H_2O mixed with 100 µl formaldehyde (30%) in 200 ml H_2O. Next, gels were washed three times for 20 s in H_2O and developed with 12 g Na_2CO_3 in 200 ml H_2O mixed with 100 µl formaldehyde (30%) until the desired staining intensity was achieved. Then, gels were washed three times for 20 s in H_2O and exposed to stop solution containing 50% ethanol and 12% acetic acid in H_2O for 3 min. A final fixation step using 5% acetic acid and 16.5% methanol in H_2O was performed for 15 min.

For Western blotting, SDS-PAGE gels were blotted onto 0.2 µm PVDF membranes using the Trans-Blot Turbo Transfer System (Bio-Rad). To improve the accessibility of epitopes, the membranes were boiled at 100 °C in PBS for 20 min, blocked in 2% BSA in PBS + 0.05% Tween-20 over night at 6 °C, washed three times with TBS + 0.05% Tween-20 + 0.1% BSA and incubated with the respective primary antibodies (Tau12, AT100 RRID:AB_223652, AT180 AB_223649) in TBS + 0.1% Tween-20 + 5% skim milk powder (Sucofin) for 2 h at room temperature. Membranes were washed three times with TBS + 0.05% Tween-20 + 0.1% BSA and incubated with anti-mouse secondary antibody conjugated to horseradish peroxidase (goat anti-mouse poly-HRP, Pierce) in TBS + 0.05% Tween-20 + 0.1% BSA for 1 h at room temperature. Membranes were washed three times with TBS + 0.05% Tween-20 + 0.1% BSA, washed once with TBS and exposed to Clarity Western ECL Substrate mixed with Peroxide solution according to manufacturer's instructions (Bio-Rad) for 5 min in the dark at room temperature. Chemiluminescent signals were detected using the ChemiDoc Touch imaging system (Bio-Rad) RRID:SCR_021693 and analyzed using Image Lab software (version 6.0) RRID:SCR_014210.

Analysis of seeding competence for SS-AD

The seeding competence of different intermediate fractions and the final SS-AD protein were assessed in a twofold dilution series using the HEK293 Tau biosensor assay as previously described [3].

For testing of SS-AD in human iPSC-derived neurons, the hiPSC line IPSC0028 (Sigma-Aldrich, Table 1) was differentiated into dorsal forebrain neural progenitors and subsequently underwent terminal differentiation to cortical excitatory hiPSC-neurons as described previously [51].

For immunocytochemistry, cells were fixed in ice-cold methanol and stained with MC1 RRID:AB_2314773 (hiPSC-derived neurons) primary antibody, kindly provided by Peter Davies to AbbVie through a Material Transfer Agreement with Feinstein Institute. Staining, imaging, and image analysis procedures have been described in detail previously [48].

Recombinant Tau aggregates

Recombinant human Tau PHFs (2 N4R P301L) were prepared as described previously [51].

Synuclein pre-formed fibrils

Wildtype full-length human α-synuclein pre-formed fibrils (PFFs) were generated as described previously [65]

and obtained from the Luk laboratory at the University of Pennsylvania [at a stock concentration of 5 mg/mL in Dulbecco's PBS (DPBS)]. PFFs were diluted to 0.1 mg/mL in Dulbecco's PBS (DPBS) and sonicated for 1 min at 30% amplitude with 1 s on, 1 s off pulses using a QSonica 500 water bath sonicator RRID:SCR_025441.

Tau aggregation assays

SI-AD and SS-AD Tau aggregation assays

Tau aggregation assays were performed as previously described [51]. Briefly, SI-AD or SS-AD protein was diluted to the appropriate concentration in neuronal maintenance media and the appropriate volume of diluted SI-AD or SS-AD protein was added to DIV16 hiPSC-neurons. Media was exchanged post-seeding on DIV19 for the first time and regular, biweekly media changes took place until DIV44. DIV44 hiPSC-neurons were fixed with ice cold 100% methanol (Sigma) at −20 °C for 15 min, followed by three PBS washes.

Tau aggregation immunofluorescence

Methanol fixed, DIV44 hiPSC-neurons were incubated with blocking buffer composed of 3% Bovine Serum Albumin (BSA) (Millipore) in PBS, for 1 h at room temperature, with shaking. Following blocking, primary antibodies were diluted in blocking buffer and filtered through a 0.22 µm Spin-X column (Corning) and added to hiPSC-neurons overnight at 4 °C, with shaking. The following day, hiPSC-neurons were washed three times with PBS and incubated with Alexa Fluor™ secondary antibody, diluted 1:500 in blocking buffer, and filtered through a 0.22 µm Spin-X column (Corning), for 1 h at room temperature, with shaking. Following secondary antibody incubation, hiPSC-neurons were incubated with Hoechst 33,342 solution (Invitrogen), diluted 1:5000 in PBS, for 15 min at room temperature, with shaking. hiPSC-neurons were subsequently washed two times with PBS and imaged on an Opera Phenix high content imaging system (PerkinElmer) RRID:SCR_021100. Quantification of MC1-positive spot area, HT7 area, and MAP2 area were performed using Harmony software (PerkinElmer) RRID:SCR_018809.

Synuclein aggregation assays

Synuclein pre-formed fibril (PFF) aggregation assays

Prior to addition to hiPSC-neuron cultures, freshly sonicated synuclein PFFs were diluted to a 2 ×concentration in prewarmed neuronal maintenance media (NMM). 2× synuclein PFFs were added at 1× to DIV21 hiPSC-neurons. hiPSC-neurons were maintained for 6 weeks following PFF addition and 1/3 media changes were performed twice weekly. After 6 weeks, hiPSC-neurons were fixed with 4% PFA (Thermo Fisher).

Synuclein aggregation immunofluorescence

PFA fixed, DIV63 hiPSC-neurons were incubated with blocking buffer composed of 3% Bovine Serum Albumin (BSA) (Millipore) in PBS, for 1 h at room temperature, with shaking. Following blocking, hiPSC-neurons were incubated with primary antibodies, diluted in blocking buffer and filtered through a 0.22 µm Spin-X column (Corning), overnight at 4 °C, with shaking. The following day, hiPSC-neurons were washed three times with PBS and incubated with Alexa Fluor™ secondary antibody, diluted 1:500 in blocking buffer and filtered through a 0.22 µm Spin-X column (Corning), for 1 h at room temperature, with shaking. Following secondary antibody incubation, hiPSC-neurons were incubated with Hoechst 33,342 solution (Invitrogen), diluted 1:5000 in PBS, for 15 min at room temperature, with shaking. hiPSC-neurons were subsequently washed two times with PBS and imaged on an Opera Phenix high content imaging system (PerkinElmer) RRID:SCR_021100.

siRNA knockdown

siRNA treatment

One day prior to transfecting hiPSC-neurons with siRNA (DIV12), hiPSC-neuron media was replaced with 100 µL NMM without penicillin and streptomycin. On DIV13, hiPSC-neurons were transfected with 25 nM Silencer Select siRNA (Thermo Fisher), using the Stemfect RNA transfection kit (Reprocell) according to manufacturer instructions. The following day, two thirds of the media was replaced with NMM without penicillin/streptomycin.

Confirmation of gene knockdown

Three days post siRNA-treatment (DIV16), hiPSC-neuron lysates were collected for total RNA isolation. RNA extraction and quantitative PCR analysis were completed as described above in "RNA isolation and quantitative PCR".

Tau aggregation assays in siRNA treated hiPSC-neurons

siRNA treated hiPSC-neurons were seeded with 0.5 nM SI-AD protein on DIV16 and methanol-fixed four weeks later (DIV44) for IF analysis.

Tau uptake and degradation analysis

pHrodo labeling of sPHFs and α-synuclein PFFs

pHrodo™ labeling was carried out with the pHrodo™ Antibody Labeling Kit (Thermo Fisher) according to manufacturer's instructions, with some modifications. Briefly, Tau sPHFs and α-synuclein PFFs were diluted to 1 mg/mL with PBS and sodium bicarbonate solution provided with the kit. Subsequently, sPHFs and PFFs were incubated with pHrodo™ red dye (freshly resuspended

to 1 mg/mL in DMSO) using a molar ratio of dye to protein of 7:1. sPHFs were incubated with dye for 30 min at room temperature, at which point 100 mM Tris HCl pH 7.5 was added to stop the dye labeling reaction. Labeled sPHFs and PFFs were then run through PD SpinTrap™ G-25 columns (Cytiva) according to manufacturer instructions to separate labeled sPHFs from remaining unbound pHrodo™ dye. Protein concentration of the resulting pHrodo™ labeled sPHFs was determined using a Micro-BCA™ Protein assay (Thermo Fisher).

Alexa Fluor 594 labeling of sPHFs for Tau uptake probe

Tau sPHFs were diluted to 1 mg/mL with 0.1M sodium bicarbonate (Sigma). A594 dye (Invitrogen) was added at a final molar ratio of 1:1 dye to protein. The sPHFs plus A594 dye were incubated for 30 min at room temperature. Labeled sPHFs were then run through PD SpinTrap™ G-25 columns (Cytiva) according to manufacturer instructions to separate labeled sPHFs from remaining unbound A594 dye. Protein concentration of the resulting A594 labeled sPHFs was determined using a Micro-BCA™ Protein assay (Thermo Fisher).

Alexa Fluor 594 plus black hole quencher labeling for Tau degradation probe

To generate the Tau degradation probe, sPHFs labeled with A594 dye were incubated with black hole quencher 3 succinimidyl ester dye (BHQ3) (Bioresearch Technologies). Briefly, BHQ3 dye was added to A594 labeled sPHFs at a 1:10 dye to protein ratio and incubated for 30 min at room temperature. Labeled sPHFs were then run through PD SpinTrap™ G-25 columns (Cytiva) according to manufacturer instructions to separate labeled sPHFs from remaining unbound A594 dye. Protein concentration of the resulting A594 and BHQ3 labeled sPHFs was determined using a Micro-BCA™ Protein assay (Thermo Fisher).

pHrodo labeled sPHF treatment and imaging

pHrodo™ labeled sPHFs were diluted in neuronal maintenance media and added to DIV16 hiPSC-neurons at a final concentration of 50 nM. Live cell images were taken at 20 × magnification every hour, starting 4 h after pHrodo™ sPHF treatment, continuing 76 h post-treatment on an Incucyte S3 (Sartorius) RRID:SCR_023147. Quantification of Tau uptake in pHrodo sPHF treated hiPSC-neurons was performed using the Incucyte S3 2018 A software RRID:SCR_023147 and normalized to TUBB3 area.

Tau uptake and degradation probe treatment and imaging

Alexa fluor 594 (A594) labeled sPHFs (Tau uptake probe) or A594 + Black hole quencher 3 (BHQ3) labeled sPHFs (Tau degradation probe) were diluted in neuronal maintenance media and added to DIV16 hiPSC-neurons at a final concentration of 50 nM. Live cell images were taken at 40 × magnification every 4 h, starting at the time of labeled sPHF addition (t = 0), using an Opera Phenix high content imaging system (PerkinElmer) RRID:SCR_021100. Quantification of A594 signal was carried out using Harmony analysis software (PerkinElmer) RRID:SCR_018809. For analysis of lysosomal dependent Tau degradation, cells were treated with 3 nM bafilomycin A1 (Sigma) at the time of Tau degradation probe addition. Lysosomal dependent degradation quantification represents the ratio of Tau degradation probe signal in hiPSC-neurons without bafilomycin A1 to the Tau degradation probe signal in hiPSC-neurons treated with bafilomycin A1. Hoechst 33,342 solution (Invitrogen) was added, at a 1:30,000 dilution, alongside fluorescently labeled sPHFs to allow visualization of nuclei. Quantification of the sum intensity of A594 spots and nuclei number were performed using Harmony software (PerkinElmer) RRID:SCR_018809.

SI-AD transfection

One day prior to SI-AD transfection (DIV15), hiPSC-neuron maintenance media was replaced by neuronal maintenance media lacking penicillin/streptomycin. On the day of seeding, SI-AD protein was diluted in a 1:10 mixture of Stemfect™ RNA transfection reagent:Stemfect™ transfection buffer (Reprocell) or an equal volume of Stemfect™ transfection buffer without Stemfect™ transfection reagent. SI-AD mixtures with or without Stemfect™ transfection reagent were incubated at room temperature for 20 min and then diluted in neuronal maintenance media to the appropriate SI-AD concentration. SI-AD with or without Stemfect™ transfection reagent was added to DIV16 hiPSC-neurons. On DIV19, the first post-seeding media exchange was performed, followed by regular biweekly media exchanges until DIV44, at which point hiPSC-neurons were methanol fixed for IF analysis.

Identification of common upregulated genes between hiPSC-neuron RNA-seq and AD brain single-nucleus-RNA-sequencing

Differential gene expression analysis was conducted on the hiPSC-neuron scRNA-seq data using a non-parametric Wilcoxon rank sum test in Seurat [50, 55] RRID:SCR_007322, comparing cortical inhibitory hiPSC-neurons vs hypothalamic hiPSC-neurons, cortical inhibitory hiPSC-neurons vs mDA hiPSC-neurons, and cortical inhibitory hiPSC-neurons vs spinal cord hiPSC-neurons. Overlapping upregulated genes from scRNA-seq comparisons were examined for overlap with upregulated

genes between the PBS-treated cortical inhibitory hiPSC-neuron vs PBS-treated hypothalamic hiPSC-neuron bulk RNA-seq analysis described above. Differential gene expression data from a published snRNA-seq data human AD brain dataset was used to identify upregulated genes in AT8-positive vs AT8-negative neurons [64]. Common upregulated genes were identified by comparing upregulated genes from the cortical inhibitory hiPSC-neurons vs resilient hiPSC-neurons and upregulated genes from the AT8-positive vs AT8-negative neurons from snRNA-seq of human AD brains. For enrichment analyses, hypergeometric tests were performed using clusterProfiler [88, 90] RRID:SCR_016884. The background gene lists list included the intersection of all genes tested for differential expression among the three datasets (hiPSC-neuron bulk RNA-seq, hiPSC-neuron snRNA-seq, and published AD brain snRNA-seq).

Statistical analysis

Statistical analyses were performed using GraphPad Prism RRID:SCR_002798. Datasets were analyzed using either a one-way ANOVA with Tukey's test (for datasets with one variable) or a two-way ANOVA with Tukey's test (for datasets with two variables). *P*-values were set as follows: * $p < 0.05$, ** $p < 0.01$, *** $p < 0.001$, **** $p < 0.0001$. Biological replicates refer to the use of different hiPSC donor lines within an experiment while technical replicates refer to independent measurements from separate wells of the same hiPSC donor line.

Figures

All figures were generated with Adobe Illustrator version 24.0 RRID:SCR_010279.

Results

Establishing hiPSC-derived neuronal models for studying selective vulnerability to Tau pathology

To determine whether different hiPSC-neuronal subtypes display unique propensities to form endogenous Tau aggregates that mimic the patterns of neuronal susceptibility observed in AD patients, we first differentiated hiPSC lines from clinically undiagnosed, apparently healthy donors into neurons expressing neuronal markers associated with either forebrain (cortical inhibitory, cortical excitatory, and hypothalamic), midbrain (midbrain dopaminergic), or hindbrain (spinal cord) identities. For our studies, 5 hiPSC donor lines were selected from individuals with differing sexes, ages, and apolipoprotein E (*APOE*) genotypes (Table 1). All hiPSC lines expressed OCT4 and NANOG, markers associated with the undifferentiated state (Supplementary Fig. 1a). The 5 hiPSC donor lines were differentiated into 5 distinct neuronal subtypes via small molecules based on established protocols [12, 21, 51, 59] (Fig. 1a). Characterization of dorsal and ventral forebrain neural progenitor cells (NPCs) indicated high expression of the neuroectoderm marker, PAX6, and low levels of common contaminants, including SOX10 (neural crest) and AP2α (non-neural ectoderm) (Supplementary Fig. 1b). Midbrain NPCs expressed OTX2 (forebrain/midbrain) and LMX1 A (midbrain) but not PAX6 while dorsal forebrain NPCs, which were PAX6-positive/OTX2-positive/LMX1 A-negative (Supplementary Fig. 1c). Spinal cord NPCs expressed OLIG2 (hindbrain) and NKX6.1 (ventral neural tube) but not FOXG1 (forebrain) or OTX2 in contrast ventral forebrain NPCs which expressed FOXG1 and OTX2 and were negative for OLIG2 and NKX6.1 (Supplementary Fig. 1d).

Following further differentiation and 21 days of subsequent neuronal maturation without replating (DIV21), the resulting neuronal populations were characterized across donor lines using a 96-gene qRT-PCR panel composed of pan-neuronal, glial, NPC, and neuron subtype-specific markers (Table 2). Principal component analysis revealed that the hiPSC-neurons largely clustered by subtype protocol and not by donor (Fig. 1b). DIV21 hiPSC-neurons expressed the pan-neuronal markers *TUBB3, MAP2, SYN1, SYP, DCX, RBFOX3* (NeuN), and *MAPT* regardless of subtype (Fig. 1c). Each neuronal subtype also expressed appropriate regional identity markers, with cortical neurons expressing *FOXG1*, the mDA neurons expressing *FOXA2, EN1, OTX2, DDC, LMX1 A,*

(See figure on next page.)

Fig. 1 Establishing hiPSC-derived neuronal models for studying selective vulnerability to Tau pathology. **a** Schematic depicting hiPSC differentiation to distinct neuronal subtypes along with their identifying marker gene expression. Created with BioRender.com. **b** PCA of DIV21 96 target gene expression data from 5 hiPSC-neuron subtypes across 5 hiPSC donor lines. The proportion of variance for PC1 is 20.73%, while the proportion of variance for PC2 is 17.04%. **c** Heat map with hierarchical clustering depicts select marker gene expression at DIV21 in 5 hiPSC-neuron subtypes across 5 hiPSC donor lines. Log10 normalized expression values are scaled per neuronal population to indicate highly expressed genes. CI = cortical inhibitory hiPSC-neurons, CE = cortical excitatory hiPSC-neurons, Hypo = hypothalamic hiPSC-neurons, mDA = midbrain dopaminergic hiPSC-neurons, SC = spinal cord hiPSC-neurons. **d** Immunofluorescence of DIV21 hiPSC-neurons differentiated to 5 distinct neuronal subtypes. Scale bar = 50 µm. **e** Quantification of DIV21 hiPSC-neuron percent of nuclei positive for cortical layer (CTIP2, TBR1) and regional identity markers (FOXG1, FOXA2, and HOXB4). **F** Western blot analysis of total Tau (TauC, red) and actin (green) from DIV16 hiPSC-neurons differentiated to 5 neuronal subtypes. L = ladder, labeled with molecular weight (kDa)

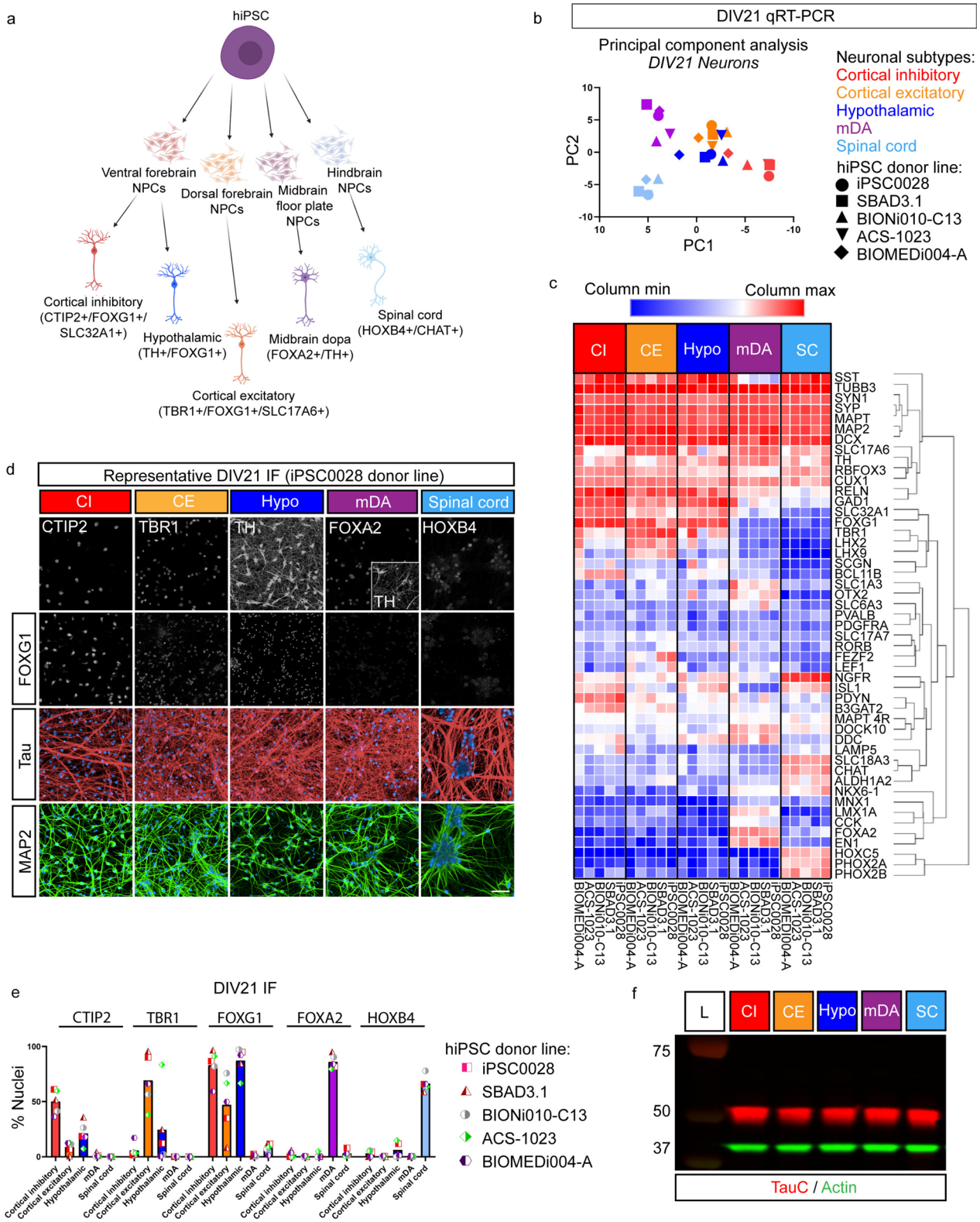

Fig. 1 (See legend on previous page.)

and *TH*, and the spinal cord neurons expressing *HOXC5, PHOX2 A, and PHOX2B*. The cortical inhibitory and cortical excitatory neurons were further separable based on their cortical layer and neurotransmitter-associated markers. Cortical inhibitory neurons expressed *BCL11B* (cortical layer V) and *SLC32 A1* (inhibitory, VGAT) while cortical excitatory neurons expressed *TBR1* (cortical layer VI) and *SLC17 A6* (excitatory, VGLUT2). While the hypothalamic neurons were derived from the same NPC intermediate as the cortical inhibitory neurons, treatment of the NPCs with SAG, FGF-8a, and BMP9 was sufficient to induce *TH* expression, which has previously been associated with a hypothalamic identity when co-expressed with *SST* [69]. mDA neurons expressed *TH*, *DDC*, and *OTX2*, consistent with a dopaminergic identity. Spinal cord neurons expressed *CHAT* and *SLC18 A3*, consistent with a cholinergic identity (Fig. 1c).

Immunofluorescence (IF) analysis was used to confirm protein expression of genes found to be differentially expressed at the RNA level, providing further confidence in the distinct identities of the hiPSC-derived neuronal subtypes (Fig. 1d and e). Representative images from a single donor line (IPSC0028) showed that cortical inhibitory hiPSC-neurons expressed the deep layer cortical marker CTIP2 (*BCL11B*), cortical excitatory hiPSC-neurons expressed the deep layer cortical excitatory marker TBR1, hypothalamic hiPSC-neurons expressed TH protein, mDA hiPSC-neurons expressed the midbrain marker FOXA2 and the dopaminergic marker TH, and spinal cord hiPSC-neurons expressed the hindbrain marker HOXB4 (Fig. 1d). scRNA-seq also showed co-expression of *BCL11B* and *SST* in hiPSC-neurons derived using the cortical inhibitory protocol, co-expression of *TBR1* and *SLC17 A6* in hiPSC-neurons derived using the cortical excitatory protocol, co-expression of FOXG1 and TH in hiPSC-neurons derived using the hypothalamic protocol, co-expression of FOXA2 and LMX1 A in hiPSC-neurons derived using the mDA protocol, and co-expression of HOXB4 and CHAT in hiPSC-neurons derived using the spinal cord-like protocol (Supplementary Fig. 2a–f). In addition, DIV21 IF quantification demonstrated the reproducibility of marker gene expression across donor lines (Fig. 1e). Consistent with observations from DIV21 qRT-PCR (Fig. 1b), the ACS-1023 hypothalamic neurons were an outlier relative to hypothalamic populations derived from other hiPSC donor lines, with a higher percentage of TBR1-positive nuclei (Fig. 1e). This provided further support to exclude the ACS-1023 hypothalamic neurons due to challenges with achieving a similar identity across donors which was critical for subsequent experiments.

Critically, while Tau and MAP2 IF staining in the hiPSC-neurons highlighted morphological differences in axonal and dendritic networks between the distinct subtypes (Fig. 1d), qPCR and western blot analysis revealed no differences in *MAPT* RNA or total Tau protein expression across the neuronal subtypes (Supplementary Fig. 1f; Fig. 2g). The maturation status of the different neuron subtypes was also evaluated by applying the neuron maturity index (NMI) [36], which showed no difference in maturation between subtypes (Supplementary Fig. 2h).

Distinct hiPSC-derived neuronal subtypes show differential susceptibility to seeding with AD brain-derived Tau aggregates

Given the spatiotemporal pattern of Tau pathology spread observed in AD, we predicted that an in vitro model that recapitulates the human disease would show that forebrain-like hiPSC-neurons display the highest vulnerability to seeding with Tau seeds (i.e. more Tau aggregation), while midbrain- and hindbrain-like hiPSC-neurons would be more resilient. We utilized an established high content Tau seeding aggregation assay to measure vulnerability to Tau in hiPSC-derived neurons [51]. This assay does not require Tau overexpression and triggers endogenous, insoluble Tau aggregation following seeding with AD brain-derived Tau without overt toxicity. hiPSC-derived neurons were seeded with sarkosyl-insoluble Tau enriched from AD brain tissue (SI-AD) at

(See figure on next page.)

Fig. 2 Distinct hiPSC-derived neuronal subtypes show differential vulnerability to seeding with AD brain-derived Tau pathology. **a** Representative DIV44 images from hiPSC-neuronal subtypes seeded with 1 nM SI-AD. MC1 labels Tau aggregates; MAP2 labels dendrites. Scale bar = 50 µm. **b** Quantification of MC1-positive spot area normalized to soluble Tau (HT7) area at DIV21 in 5 hiPSC-neuron subtypes across 5 donor lines, seeded with range of SI-AD concentrations. Data normalized to cortical inhibitory hiPSC-neurons seeded with 1 nM SI-AD. Data represents the average of 4 or 5 biological replicates + SD (3 technical replicate wells, 30 fields per well). ns = not significant, * = *p*-value < 0.05, ** = *p*-value < 0.01, *** = *p*-value < 0.001, **** = *p*-value < 0.0001 according to one-way ANOVA with Tukey's test. **c** Representative DIV44 images from unseeded hiPSC-neurons (left) or hiPSC-neuronal subtypes seeded with 1 nM SS-AD. MC1 labels tau aggregates; MAP2 labels dendrites. Scale bar = 50 µm**. d** Quantification of MC1-positive spot area normalized to soluble Tau (HT7) area at DIV21 in 5 hiPSC-neuron subtypes across 3 donor lines, seeded with range of SS-AD concentrations. Data normalized to cortical inhibitory hiPSC-neurons seeded with 1 nM SI-AD. Data represents the average of 2 or 3 biological replicates + SD (3 technical replicate wells, 30 fields per well). ns = not significant, ** = *p*-value < 0.01 according to one-way ANOVA with Tukey's test

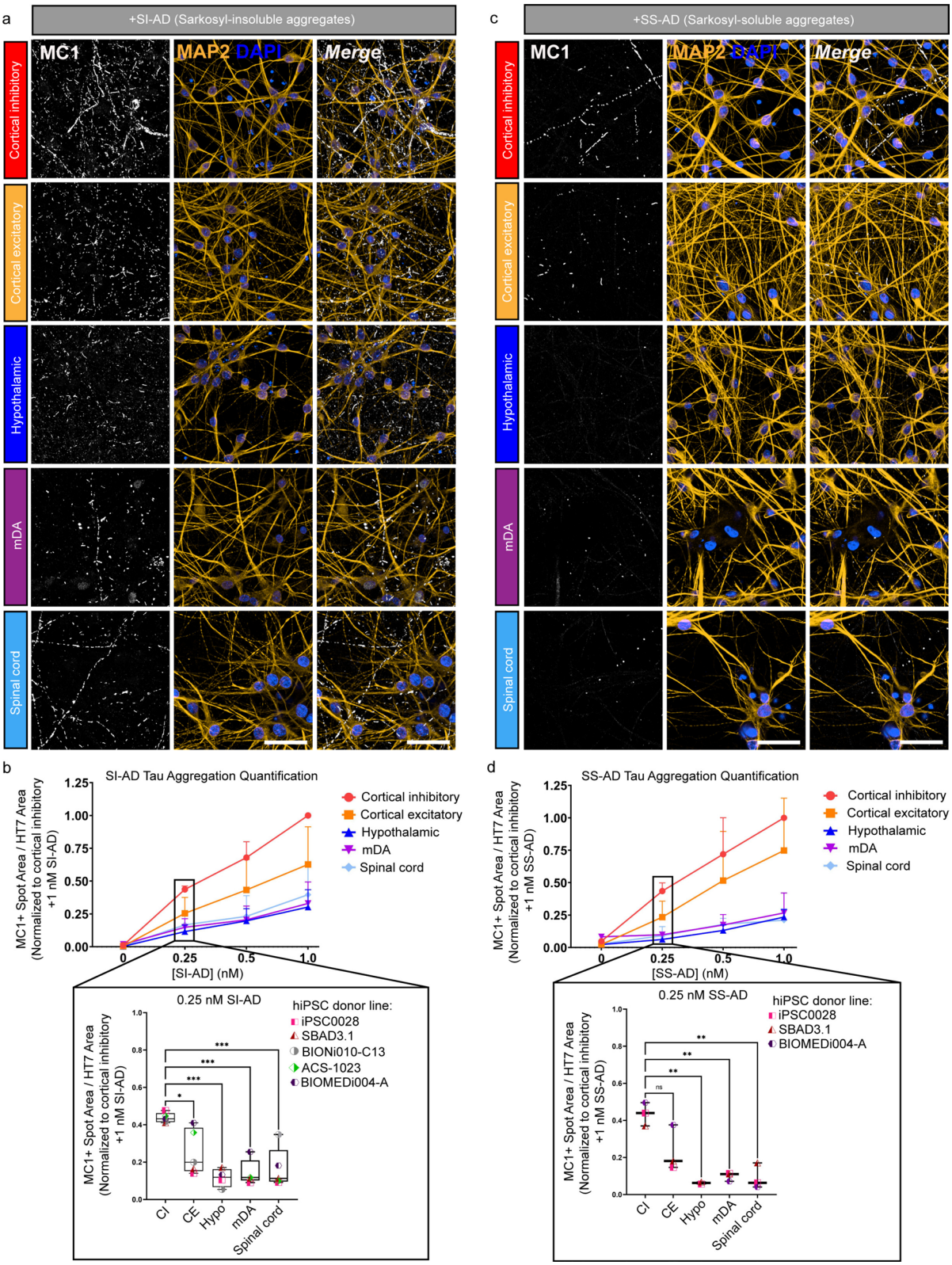

Fig. 2 (See legend on previous page.)

0.25, 0.5, or 1 nM on DIV16 (i.e. 16 days after neuron maturation in the final assay plate). Four weeks post treatment [51], cells were fixed with methanol to remove soluble Tau and endogenous Tau aggregation was quantified using IF labeling with MC1, a conformation-specific antibody against pathological Tau [40], followed by high content imaging. MC1 immunoreactivity in hiPSC-neurons 4 weeks post exogenous Tau aggregate addition revealed the presence of endogenous Tau aggregates triggered by the application of SI-AD material (Fig. 2a). Quantification of MC1-positive insoluble Tau aggregates revealed that the cortical inhibitory neurons consistently displayed the most Tau aggregation among the neuron subtypes tested and across donor lines (Fig. 2a and b, Supplementary Fig. 3). In contrast, the cortical excitatory, hypothalamic, mDA, and spinal cord neurons showed lower levels of Tau aggregation relative to the cortical inhibitory neurons. Interestingly, the TBR1-positive cortical excitatory neurons showed more variability in their relative Tau aggregation levels across donor lines, with the cortical excitatory neurons derived from the ACS-1023 and BIOMEDi004-A donors having more similar aggregation relative to their respective cortical inhibitory neurons.

We then investigated whether the susceptibility to Tau aggregation was influenced by the type of seeding-competent Tau species used. For this purpose, we isolated sarkosyl soluble Tau aggregates (SS-AD) from AD-brain [45]. While SI-AD is believed to represent neurofibrillary tangle brain deposits, SS-AD contains smaller soluble Tau aggregates more likely to be responsible for the propagation and spread of Tau pathology from neuron to neuron in AD-brain [28] (for a detailed description of biochemical and seeding properties of SS-AD, see Supplementary Fig. 4). While SS-AD triggered lower total Tau aggregation relative to SI-AD (Fig. 2c), SS-AD seeding led to a similar pattern of relative Tau aggregation levels observed with SI-AD seeding. CTIP2-positive SST-positive cortical inhibitory hiPSC-neurons consistently showed the highest relative Tau aggregation levels, while hypothalamic, mDA, and spinal cord hiPSC-neurons showed lower relative Tau aggregation levels on average (Fig. 2c and d, Supplementary Fig. 5). Similar to our findings with SI-AD, cortical excitatory neurons seeded with SS-AD showed higher donor line variability in their Tau aggregation outcome relative to other neuronal subtypes, with the cortical excitatory neurons derived from the BIOMEDi004-A donor having more similar aggregation relative to their respective cortical inhibitory neurons (Fig. 2c). Taken together, these data suggest that the pattern of susceptibility to Tau aggregation is independent of a specific pathological Tau fraction contained in the seeding material.

Finally, we evaluated whether the ability of hiPSC-neurons to exhibit differential susceptibility is unique to seeding with Tau. While Tau pathology affects forebrain neurons early in AD, aggregated α-synuclein which gives rise to Lewy bodies, the pathological hallmark of PD, occurs earlier in mDA neurons as compared to forebrain neurons [31]. In line with this pattern of vulnerability, Brazdis et al. found that mDA hiPSC-neurons derived from a donor line carrying a *SNCA* duplication associated with familial PD show increased α-synuclein aggregation and higher susceptibility to α-synuclein toxicity relative to cortical hiPSC-neurons derived from the same donor line [9]. Here, we used α-synuclein pre-formed fibrils (PFFs), which are capable of seeding aggregation of endogenous α-synuclein in vitro and in vivo [14], to test the inherent susceptibility of hiPSC-neurons to these exogenous aggregates. α-synuclein PFFs were added to hiPSC-neurons matured for 21 days. Consistent with the patterns of vulnerability observed in PD, seeding with PFFs resulted in a concentration-dependent increase in pS129 α-synuclein, a marker of aggregated α-synuclein [27], in mDA hiPSC-derived neurons (Supplementary Fig. 6a and b). In contrast, cortical excitatory hiPSC-neurons seeded with α-synuclein PFFs displayed almost no detectable pS129 α-synuclein relative to mDA hiPSC-neurons despite similar expression levels of *SNCA* (Supplementary Fig. 6a–c). These findings further support the dependence of aggregation propensity on the compatibility between the aggregated exogenous protein and the neuronal subtype.

Exogenous aggregate uptake is similar across neuronal subtypes

One possible explanation for the differences observed in aggregation load between neuronal subtypes could be differences in uptake of the exogenous aggregates. To this end, we examined exogenous Tau uptake rates in the distinct neuronal subtypes using pHrodo 568, a pH sensitive dye that enables measurement of a fluorescent signal triggered by entry into acidic cellular compartments, such as the endosome or lysosome, over time. Attempts to label SI-AD or MC1-immunopurified AD (MC1-AD) material were unsuccessful, likely due to the low concentration of Tau as well as the relative impurity in SI-AD and MC1-AD (data not shown). As a suitable pure alternative, sonicated 2N4R P301L recombinant Tau PHF (sPHF) were labeled with pHrodo dye as performed previously [22] and hiPSC-derived neurons were treated with 50 nM pHrodo-labeled sPHF. Unexpectedly, subtypes more resilient to forming Tau aggregates, including mDA and spinal cord-like neurons, showed accelerated sPHF uptake relative to the highly vulnerable cortical inhibitory neurons (Supplementary Fig. 7a and b). Similarly,

we measured pHrodo-labeled α-synuclein PFF uptake in mDA and cortical excitatory hiPSC-derived neurons to determine whether uptake rates contribute to the selective vulnerability of mDA neurons to α- synuclein PFFs. No differences were observed in recombinant monomeric α-synuclein or α-synuclein PFF uptake rates between the vulnerable mDA-like neurons and the more resilient cortical-like neurons (Supplementary Fig. 7c).

Since pHrodo dye emission increases in acidic environments, we wondered if the results could suggest a higher lysosomal degradation rate of sPHF rather than a difference in sPHF uptake. To distinguish between uptake and degradation rates, we utilized a non-pH sensitive fluorescent dye, Alexa Fluor 594 (A594), in combination with a quencher. sPHF labeled with A594 and the quencher (QA594 sPHF) produce a fluorescent signal only when the labeled sPHF is degraded, releasing the quencher from the fluorescent dye (Fig. 3a). Therefore, sPHF labeled only with A594 (A594 sPHF) could be used to measure Tau uptake rates, while QA594 sPHF could be used to measure degradation rates. Results obtained using A594 sPHF were consistent with pHrodo-labeled sPHF data, with more Tau-resilient subtypes (the spinal cord and mDA neurons) showing higher uptake rates and more total uptake than the more Tau-vulnerable subtype (cortical inhibitory neurons) (Fig. 3b). Interestingly, hypothalamic neurons, which have a low susceptibility to forming Tau aggregates, displayed similar rates of sPHF uptake and total uptake compared to the highly vulnerable cortical inhibitory neurons (Fig. 3b and c). Spinal cord and mDA neurons also showed the highest QA594 signal, consistent with a higher rate of Tau degradation. However, only the spinal cord neurons showed an increased rate of sPHF degradation when data was normalized to sPHF uptake (Fig. 3d). Spinal cord neurons are also the only neuronal subtype tested which showed an increase in lysosomal dependent degradation, which measures the change in sPHF degradation in the presence of the lysosomal deacidifier, bafilomycin A1 (Fig. 3e). These data suggest that while differences in degradation of Tau aggregates may partially explain the resilience of the spinal cord-like neurons, enhanced degradation is not likely a universal mechanism or the only mechanism to confer resilience.

Because efforts to label SI-AD with dyes were unsuccessful and sPHF does not induce aggregation of endogenous Tau in hiPSC-neurons expressing wild-type Tau [51], we then asked whether bypassing endogenous Tau aggregate uptake pathways could confirm our finding that the differences in susceptibility to form Tau pathology cannot simply be explained by differences in Tau aggregate uptake alone. To this end, SI-AD material was packaged in lipid components to enable passive transport across the plasma membrane similar to the route of Tau seeding used in HEK cells [37]. In all neuronal subtypes tested, lipid-assisted seeding increased the levels of Tau aggregation (Fig. 3f). Interestingly, the Tau aggregation was impacted mostly in spinal cord neurons (ratio of transfected to untransfected Tau aggregation is ~4; Fig. 3g); however, the increase was not enough to be on par with cortical inhibitory neurons (CI = 2.1 vs spinal cord = 1.3) (Fig. 3f), suggesting that additional mechanisms contribute to the different abilities to form Tau aggregates.

RAB7 A genetic knockdown increases seeded Tau aggregation across neuronal subtypes

Another possible explanation for differential susceptibility across neuronal subtypes could be differences in endosomal trafficking of exogenous Tau aggregates

(See figure on next page.)

Fig. 3 Comparing Tau seed uptake and degradation across distinct hiPSC-neuron subtypes. **a** Sonicated paired helical filaments (sPHFs, 2 N4R P301L) labeled with Tau uptake probe (A594, not depicted in schematic) or Tau degradation probe (QA594, example shown in schematic) produce a fluorescent signal following hiPSC-neuron uptake (A594 rPHFs) or intracellular degradation (QA594 rPHFs). Adapted from "Cellular Uptake of MIL-89 Nanoparticles into Endocytic Vesicles", by BioRender.com (2024). **b** Quantification of Tau uptake normalized to nuclei count over a 12-h timecourse (*left*) and at the final timepoint (*right*) in DIV16 hiPSC-neurons treated with 50 nM A594 sPHFs (Tau uptake probe). Data represents the mean + SD (3 technical replicate wells, 12 fields per well). * = *p*-value < 0.05, ** = *p*-value < 0.01, **** = *p*-value < 0.0001 according to one-way ANOVA with Tukey's test. **c** Representative live cell images of Tau uptake in DIV16 hiPSC-neurons 12 h post-treatment with 50 nM A594 sPHFs (tau uptake probe). 594 fluorescence represents sPHF uptake, nuclei stained with Hoechst dye. Scale bar = 50 µm. **d** Ratio of Tau degradation to Tau uptake in DIV16 hiPSC-neurons 12 h post-treatment with 50 nM QA594 sPHFs (Tau degradation probe). Data represents the mean + SD (3 technical replicate wells, 12 fields per well). ** = *p*-value < 0.01, *** = *p*-value < 0.001 according to one-way ANOVA with Tukey's test. **e** Quantification of Tau degradation normalized to Tau degradation in BafA1 pretreated DIV16 hiPSC-neurons 12 h post-treatment with 50 nM QA594 sPHFs (tau degradation probe). Data represents the mean + SD (3 technical replicate wells, 12 fields per well). * = *p*-value < 0.05, ** = *p*-value < 0.01, *** = *p*-value < 0.001 according to one-way ANOVA with Tukey's test. **f** Quantification of MC1-positive spot area normalized to HT7 area in DIV44 hiPSC-neurons seeded with 0.5 nM SI-AD alone or in combination with StemFect. Data represents the mean + SD (3 technical replicate wells, 20 fields per well). **g** Ratio of transfected Tau aggregation to untransfected Tau aggregation in DIV44 hiPSC-neurons seeded with 0.5 nM SI-AD alone (untransfected) or in combination with StemFect (transfected). Data represents the mean + SD (3 technical replicate wells, 20 fields per well). Dotted line indicates a 1:1 ratio. * = *p*-value < 0.05 according to one-way ANOVA with Tukey's test

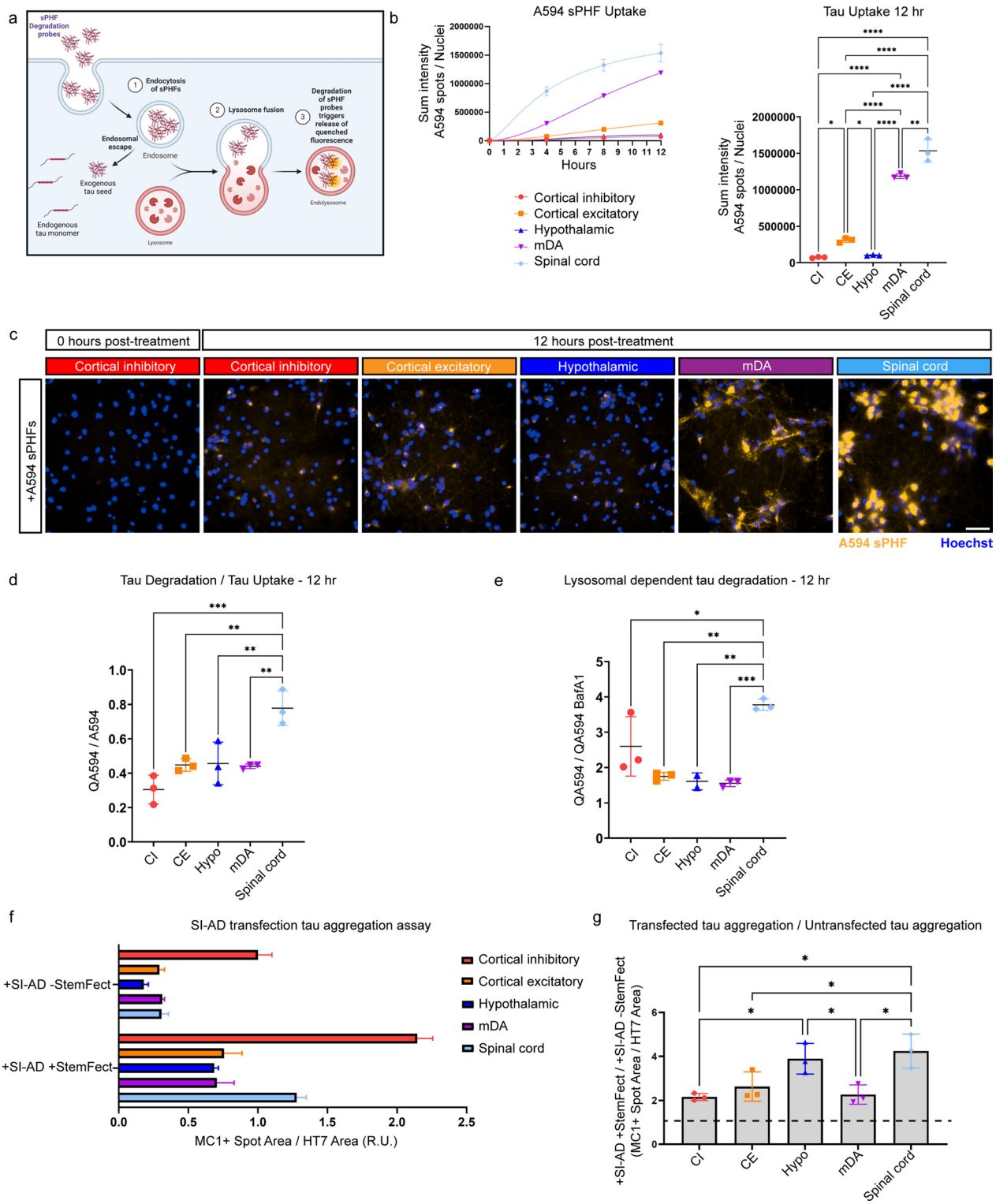

Fig. 3 (See legend on previous page.)

as a mediator of aggregation [13, 78]. To this end, we examined whether impairing the endosomal system via *RAB7 A* genetic knockdown [38, 79, 81, 89] would preferentially affect aggregation levels in a subset of our 5 hiPSC-derived neuronal subtypes where Tau aggregates may be more rapidly degraded. Equivalent levels of

RAB7 A expression were detected by scRNA-seq across all subtypes, indicating no inherent differences between Tau-vulnerable and Tau-resilient neurons and no heterogeneity within each differentiation protocol (Fig. 4a). siRNA knock down of *RAB7 A* prior to SI-AD treatment reduced *RAB7 A* mRNA by more than 90% relative to non-targeting control (NTC) siRNA (Supplementary Fig. 8a). Knockdown of *RAB7 A* significantly increased MC1-positive Tau aggregation levels relative to NTC siRNA in all subtypes except the mDA neurons where a trend was still observed (Fig. 4b and c). Surprisingly, the increased Tau aggregation observed with *RAB7 A* knockdown was not associated with decreased sPHF degradation rates (i.e. more endosomal escape) 12 h post-seeding in the majority of hiPSC-neuron subtypes as measured by QA594 fluorescence, except for a modest, but statistically significant, decrease in spinal cord hiPSC-neurons with one of two *RAB7 A* siRNAs (s15442) (Supplementary Fig. 8b).

3.5. Bulk RNA-seq identifies basal transcriptional differences between a vulnerable and resilient neuronal subtype but no consistent transcriptional changes following SI-AD treatment.

We next asked whether hiPSC-derived neurons with differential susceptibility to forming Tau aggregates have unique transcriptional responses to seed-induced Tau aggregation. We selected the cortical inhibitory and hypothalamic neuron subtypes based on their highly contrasting susceptibility to Tau aggregation despite their derivation from the same neural progenitor cell population (Fig. 1a) to minimize differential expression due to the unique neuronal identities and based on their similar Tau aggregate uptake properties (Fig. 3b). The neurons were treated with SI-AD, sarkosyl-insoluble extracts prepared from control donor brains (SI-control [51]), or PBS for 72 h and then subjected to bulk RNA-seq (Fig. 5a). We did not detect consistent transcriptional changes with SI-AD treatment relative to seeding with SI-control in either cortical inhibitory or hypothalamic neurons derived from three donor lines (Fig. 5b, Supplementary Fig. 9a). Furthermore, any non-significant changes observed showed a similar trend in both SI-AD- and SI-control-treated hiPSC-neurons relative to PBS-treated hiPSC-neurons (Supplementary Fig. 9a), suggesting a response to protein added that was not specific to Tau. A lack of consistent transcriptional changes was also observed in hiPSC-derived neurons collected 1-, 2-, and 3 weeks post SI-AD seeding and in hiPSC-neurons treated with α-synuclein PFFs relative to hiPSC-neurons treated with α-synuclein monomer (data not shown). Taken together, these findings suggest that an overt transcriptional response to aggregate seeding does not underly the differences in aggregation propensity in the in vitro model.

Next, we focused on baseline transcriptional differences between the neuronal subtypes in the control (PBS-treated) condition to define a signature of intrinsic baseline properties that could be interrogated to identify genes that confer differential susceptibility to Tau aggregation. We identified 2,855 upregulated genes and 2,353 downregulated genes in cortical inhibitory neurons relative to hypothalamic neurons that were shared across the 3 donor lines (Fig. 5c and d, Supplementary Fig. 9b, Additional File 1). Enrichment analysis of the common downregulated genes in cortical inhibitory hiPSC-neurons relative to hypothalamic hiPSC-neurons showed significant enrichment of peptidase inhibitor, peptidase regulator, and endopeptidase inhibitor activity pathways (Supplementary Fig. 9c). Studies have demonstrated Tau cleavage by peptidases and this process has been proposed to favor Tau aggregation [67, 91]. Further, Tau fragments are associated with the pronase resistant core of AD PHF [85] and certain Tau fragments in the cerebrospinal fluid (CSF) could have utility for discriminating AD patients from control [15, 42]. Genes downregulated in Tau-vulnerable cortical inhibitory hiPSC-neurons relative to Tau-resilient hypothalamic hiPSC-neurons also showed enrichment of genes related to cell–cell adhesion, cadherin binding, and integrin binding (Supplementary Fig. 9c). Genes in these pathways have functions related to intercellular contact (*ANXA1*, *ANXA2*, *CDC42EP1*, *CNN3*, *PDLIM1, PDLIM5*) (Additional File 2), which has been shown to play a role in the spread of Tau aggregates [10, 82].

(See figure on next page.)

Fig. 4 *RAB7 A* genetic knockdown increases seeded tau aggregation across neuronal subtypes. **a** UMAP visualization of single cell RNA-seq (scRNA-seq) data generated from DIV14 hiPSC-neurons colored by protocol (top) or by *RAB7 A* expression (bottom). **b** Representative DIV44 images from SI-AD seeded hiPSC-neurons pre-treated with non-targeting control (NTC) siRNA or *RAB7 A* siRNA. MC1 labels tau aggregates; MAP2 labels dendrites. Scale bar = 50 µm. **c** Quantification of MC1-positive spot area normalized to MAP2 area in hiPSC-neurons seeded with 0.5 nM SI-AD following treatment with non-targeting control (NTC) or either of two individual (non-pooled) *RAB7 A* siRNA. Data normalized to cortical inhibitory hiPSC-neurons treated with NTC siRNA. Data represents the mean + SD (3 technical replicate wells, 20 fields per well). ns = not significant, * = *p*-value < 0.05, ** = *p*-value < 0.01, *** = *p*-value < 0.001, **** = *p*-value < 0.0001 according to two-way ANOVA with Tukey's test

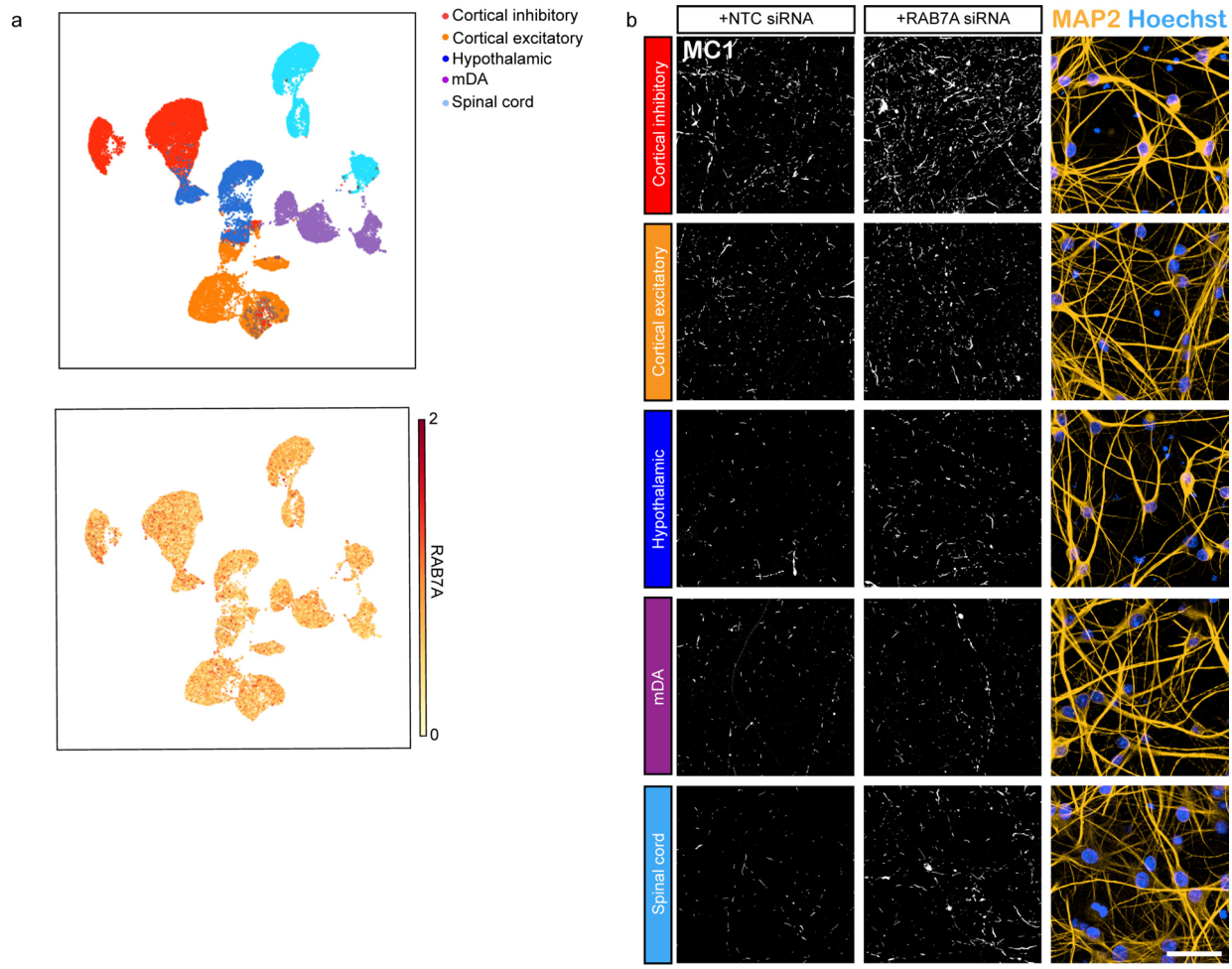

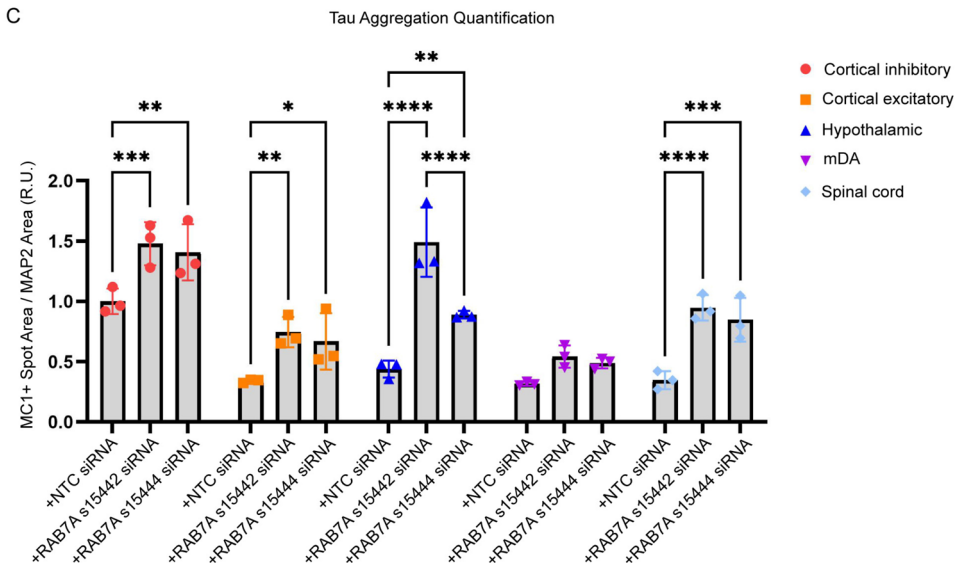

Fig. 4 (See legend on previous page.)

Enrichment analysis of the common upregulated genes in cortical inhibitory relative to hypothalamic neurons showed significant enrichment of pathways related to ion transport (Fig. 5e). Among the differentially expressed genes related to ion transport, a number encode for voltage-gated calcium channel subunits (*CACNA1G*, *CACNA1H*, *CACNA1I*, *CACNA2D1*, *CACNA2D2*, *CACNA2D3*, *CACNB4*, *CACNG2*, *CACNG3*, *CACNG5*, *CACNG7*, *CACNG8*), voltage-gated sodium channel subunits (*SCN2B*, *SCN3B*, *SCN4 A*, *SCN8 A*, *SCNN1D)* and voltage-gated potassium channel subunits (*KCNA1*, *KCNA2*, *KCNA4, KCNAB1, KCNAB2, KCNAB3, KCNC2, KCND1, KCND2, KCNF1, KCNG3, KCNH2, KCNH, KCNIP2, KCNIP3*) (Additional File 3). Upregulated genes in Tau-vulnerable hiPSC-neurons also encode subunits of Ca2 + ATPases (*ATP2B2, ATP2B3*) and Na +/K + -ATPases (*ATP1 A1, ATP1B2*) (Additional File 3). Additionally, the analysis highlighted significant enrichment of pathways related to synapse homeostasis (Fig. 5f). Protein products of upregulated genes related to the presynapse and neuronal communication contribute to neurotransmitter response (*NTSR1, P2RY1, GRM4*, *GRM5*) and exocytosis regulation (*SYNGR1, SNPH*, *SYT7*, *DGKI*) (Additional File 3). Two presynapse-associated genes upregulated in cortical inhibitory neurons encode the native proteins of pathological aggregates in Huntington's disease (*HTT*; huntingtin) and Parkinson's disease (*SNCA*; α-synuclein). Upregulated genes associated with postsynapse-related pathways in this analysis include GABA-A receptor gene family members (*GABRA1*, *GABRA4*, *GABRA5*, *GABRB2*), the SLC8 gene family of sodium-calcium exchangers (*SLC8 A1*, *SLC8 A2*, *SLC8 A3*), and genes such as *DLG4* and *CAMK2 A* (Additional File 3).

We next used SynGO, an expertly curated, public database designed for analyzing synapse biology [44], to gain further insight into synaptic gene expression changes in our dataset. Of the 2,855 upregulated genes in cortical inhibitory neurons relative to hypothalamic neurons shared across the 3 donor lines, 325 genes mapped to SynGO annotated genes (Fig. 5g and h, Supplementary Fig. 10). When looking at cellular compartment annotations of the 325 SynGO genes upregulated in vulnerable cortical inhibitory relative to resilient hypothalamic hiPSC-neurons, 53 genes had a 'postsynapse' annotation, 34 genes had a 'presynapse' annotation, and 5 genes had the annotation 'integral component of synaptic membrane' (Fig. 5g). The 325 differentially expressed synaptic genes fell into a broad range of biological process categories. The categories with the most differentially expressed genes included 'modulation of chemical synaptic transmission' with 24 genes, 'regulation of postsynapse assembly' with 14 genes, and 'regulation of postsynapse organization' with 14 genes (Fig. 5h). Of the numerous baseline transcriptional differences observed between Tau-vulnerable cortical inhibitory hiPSC-neurons and Tau-resilient hypothalamic hiPSC-neurons, differences in synaptic gene expression may be particularly relevant to the observed Tau aggregation outcomes in our in vitro system, based on substantial evidence from the literature demonstrating aggregated Tau propagation between synaptically-connected neurons [10, 19, 30, 82].

Among the differentially expressed genes identified via bulk RNA-seq, *COL25 A1* was highly upregulated in cortical inhibitory neurons relative to hypothalamic neurons (Supplementary Fig. 11a). *COL25 A1* was also found via scRNA-seq of the 5 neuronal subtypes from a single donor to be highly enriched in the CTIP2-positive, (*BCL11B)* SST-positive cortical inhibitory neurons

(See figure on next page.)

Fig. 5 Bulk RNA-seq identifies basal transcriptional differences between a vulnerable and resilient neuronal subtype, while revealing no consistent transcriptional changes following SI-AD treatment. **a** Timeline for bulk RNA-seq experiments examining transcriptional responses to SI-AD treatment in vulnerable (cortical inhibitory) and resilient (hypothalamic) hiPSC-neurons. DIV16 hiPSC-neurons were treated with PBS, SI-control, or SI-AD (0.5 nM) for 72 h prior to lysate collection for bulk RNA-seq. Created with BioRender.com. **b** Representative volcano plots showing Log(2)FC and -Log(10) adjusted *P*-values from bulk RNA-seq comparison between SI-AD treated (0.5 nM) and SI-control treated (equal volume) hiPSC-neurons in the iPSC0028 donor line. **c** Volcano plot of differentially expressed genes in PBS-treated cortical inhibitory and hypothalamic hiPSC-neurons derived from the iPSC0028 donor line. Log_2FC threshold > 1 and adj.P.val < 0.05. **d** Venn diagram showing the number of overlapping upregulated genes between DIV19 PBS-treated cortical inhibitory and hypothalamic hiPSC-neurons across hiPSC donor lines. **e** Top 25 enriched GO molecular functions for common upregulated genes in DIV19 cortical inhibitory vs hypothalamic hiPSC-neurons across hiPSC donor lines, enrichment *p*-value < 0.05. Count refers to the number of differentially expressed genes from each GO molecular function. Circle color represents adjusted *p*-value. **f** Top 25 enriched GO cellular compartments for common upregulated genes in DIV19 cortical inhibitory vs hypothalamic hiPSC-neurons across hiPSC donor lines, enrichment *p*-value < 0.05. Count refers to the number of differentially expressed genes from each GO biological process. Circle color represents adjusted *p*-value. **g** Sunburst plot of SynGO annotated cellular component synaptic genes which are upregulated in PBS-treated DIV19 cortical inhibitory vs hypothalamic hiPSC-neuron bulk RNA-seq analysis. Plot is colored by gene count per term. Gene categories mentioned in the text are outlined in yellow and labeled. **h** Sunburst plot of SynGO annotated biological process synaptic genes which are upregulated in PBS-treated DIV19 cortical inhibitory vs hypothalamic hiPSC-neuron bulk RNA-seq analysis. Plot is colored by gene count per term. Gene categories mentioned in the text are outlined in yellow and labeled with numbers

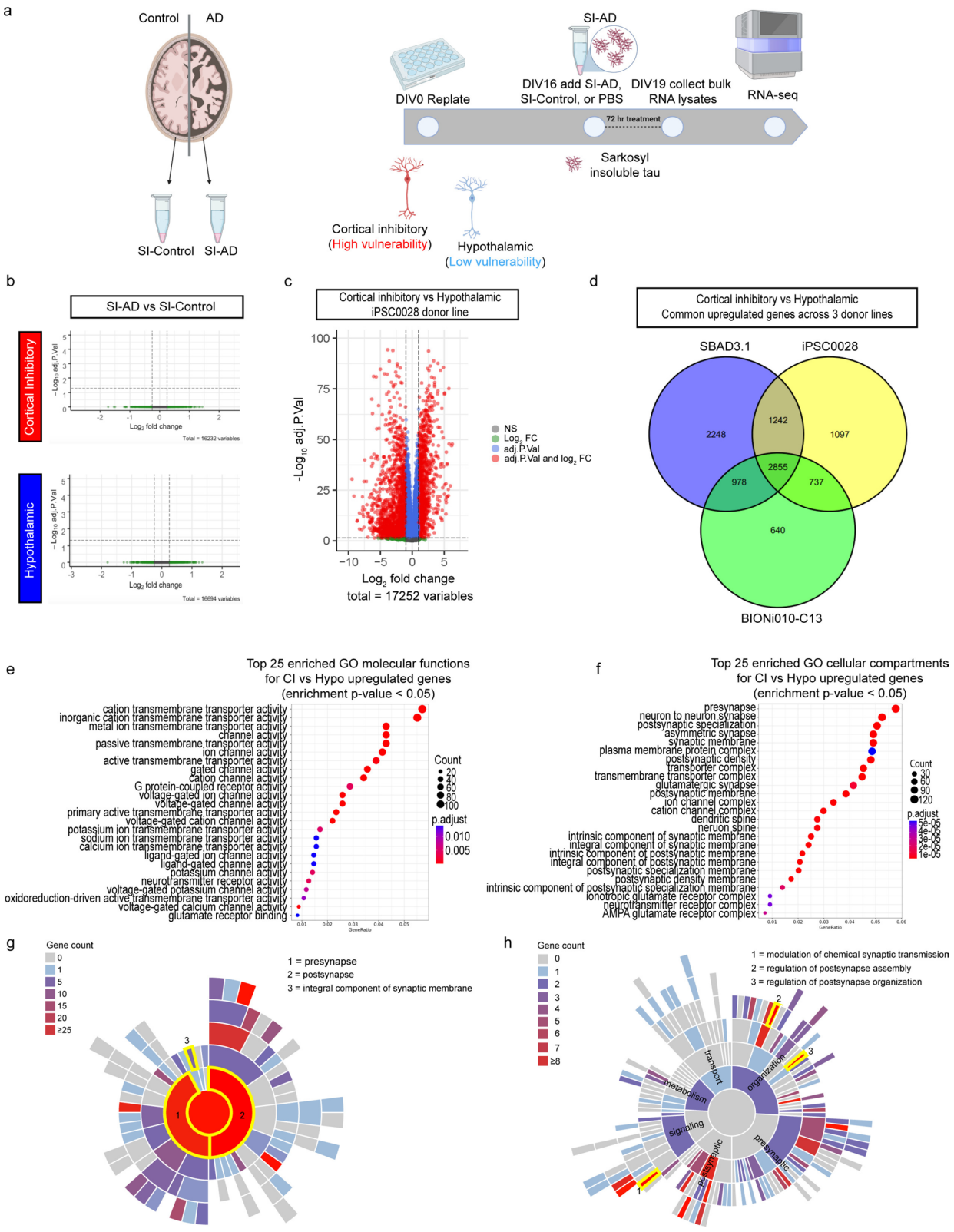

Fig. 5 (See legend on previous page.)

relative to cortical excitatory, spinal cord, hypothalamic, and mDA-like neurons derived from a single hiPSC donor line (Supplementary Fig. 11b). *COL25 A1* encodes the collagen-like Alzheimer amyloid plaque component (CLAC) protein which was identified due to its association with amyloid plaques [35]. Further, single nucleotide polymorphisms (SNPs) in the *COL25 A1* gene are associated with an increased risk for AD [24]. To determine whether *COL25 A1* is a driver of susceptibility to Tau aggregation in cortical inhibitory neurons, siRNA knockdown was performed. Three days prior to Tau seeding, three individual siRNAs targeting *COL25 A1* were transfected into cortical inhibitory neurons, resulting in 55%, 49%, or 66% reduction of *COL25 A1* expression at the RNA level on the day of seeding compared to neurons transfected with a NTC siRNA (Supplementary Fig. 11c). Following seeding, cortical inhibitory neurons were cultured for 4 weeks to allow development of Tau aggregates prior to high content imaging analysis of aggregation load via MC1 immunofluorescence labeling. Despite significant RNA knockdown, *COL25 A1* knockdown in the cortical inhibitory neurons had no effect on the Tau aggregation level induced by SI-AD seeding (Supplementary Fig. 11d).

To broaden our approach to identifying genes which may contribute to selective vulnerability by further linking the expression changes to changes found in AD, we devised a funneling strategy to look for overlap between genes differentially expressed in our hiPSC-neurons and genes differentially expressed in tangle-bearing neurons found in AD brain tissue [64] (Fig. 6a-b). Otero-Garcia and colleagues used fluorescence activated cell sorting (FACS) to isolate neuron somas with NFTs from AD brain tissue followed by snRNA-seq to evaluate gene expression profiles associated with neurons bearing AT8-positive pathological Tau aggregates [64]. First, to increase the confidence in the differentially expressed genes between our vulnerable cortical inhibitory hiPSC-neurons and more resilient hypothalamic hiPSC-neurons, we identified overlap of genes also upregulated in cortical inhibitory hiPSC-neuron scRNA-seq relative to three resilient hiPSC-neuron subtypes (hypothalamic, mDA, and spinal cord). Of the 2,855 common, upregulated genes in our bulk RNA-seq analysis of the vulnerable cortical inhibitory neurons relative to the more resilient hypothalamic neurons, 628 genes were also upregulated in the cortical inhibitory neuron scRNA-seq relative to the three resilient hiPSC-neuron subtypes (hypothalamic, mDA, and spinal cord) (Fig. 6a). Of the 628 genes, 116 genes were also upregulated in NFT-bearing neurons identified by Otero-Garcia et al. (Fig. 6c; Additional File 4). Of the 335 common downregulated genes in tau-vulnerable relative to tau-resilient hiPSC-neurons (Fig. 6b), 14 genes were also downregulated in NFT-bearing neurons identified by Otero-Garcia et al. (Fig. 6d; Additional File 5). We performed enrichment analysis on the 116 overlapping upregulated genes and found significant enrichment of pathways related to synapse homeostasis, membrane potential, and ion transport, among others (Fig. 6e). Top enriched GO terms included synaptic signaling, chemical synaptic transmission, ion transmembrane transport, cation transport,

(See figure on next page.)

Fig. 6 Identifying transcriptomic signatures of selective vulnerability to Tau aggregation. **a** Funneling strategy to identify overlapping upregulated genes between our Tau-vulnerable cortical inhibitory hiPSC-neurons relative to Tau-resilient hypothalamic hiPSC-neurons and AT8-positive vs AT8-negative neurons from Otero-Garcia et al. [64]. The 2855 genes found to be upregulated in DIV19 cortical inhibitory hiPSC-neurons relative to hypothalamic hiPSC-neurons via bulk RNA-seq was narrowed to 628 gene candidates by looking for overlapping, upregulated genes from the single cell RNA-seq analysis of cortical inhibitory hiPSC-neuron gene expression relative to resilient hiPSC-neuron gene expression (hypothalamic, mDA, and spinal cord). The list of 628 genes upregulated in cortical inhibitory hiPSC-neurons relative to resilient hiPSC-neuron subtypes identified via bulk and single cell RNA-seq was then compared to the upregulated genes in AT8-positive human AD neurons from Otero-Garcia et al. (2022). The funneling strategy identified 116 genes for follow-up analyses. **b** Funneling strategy to identify overlapping downregulated genes between our Tau-vulnerable cortical inhibitory hiPSC-neurons relative to Tau-resilient hypothalamic hiPSC-neurons and AT8-positive vs AT8-negative neurons from Otero-Garcia et al. [64]. The 2353 genes found to be downregulated in DIV19 cortical inhibitory hiPSC-neurons relative to hypothalamic hiPSC-neurons via bulk RNA-seq was narrowed to 335 gene candidates by looking for overlapping, downregulated genes from the single cell RNA-seq analysis of cortical inhibitory hiPSC-neuron gene expression relative to resilient hiPSC-neuron gene expression (hypothalamic, mDA, and spinal cord). The list of 335 genes downregulated in cortical inhibitory hiPSC-neurons relative to resilient hiPSC-neuron subtypes identified via bulk and single cell RNA-seq was then compared to the downregulated genes in AT8 human AD neurons from Otero-Garcia et al. [64]. The funneling strategy identified 14 genes, too few to run follow-up enrichment analyses. **c** Venn diagram depicting the overlapping upregulated genes from our studies on tau-vulnerable hiPSC-neurons relative to tau-resilient hiPSC-neurons and from AT8-positive vs AT8-negative neurons from Otero-Garcia et al. [64] **d** Venn diagram depicting the overlapping downregulated genes from our studies on tau-vulnerable hiPSC-neurons relative to tau-resilient hiPSC-neurons and from AT8-positive vs AT8-negative neurons from Otero-Garcia et al. [64]. **e** Pathway enrichment analysis visualization for top 25 enriched GO terms for the 116 genes identified as upregulated in both vulnerable hiPSC-neurons relative to resilient hiPSC-neurons and in AT8-positive vs AT8-negative human AD neurons, enrichment p-value < 0.05. Lines between pathways represent overlapping genes between pathways. Number of genes refers to the number of differentially expressed genes from each GO term. Circle color represents adjusted p-value

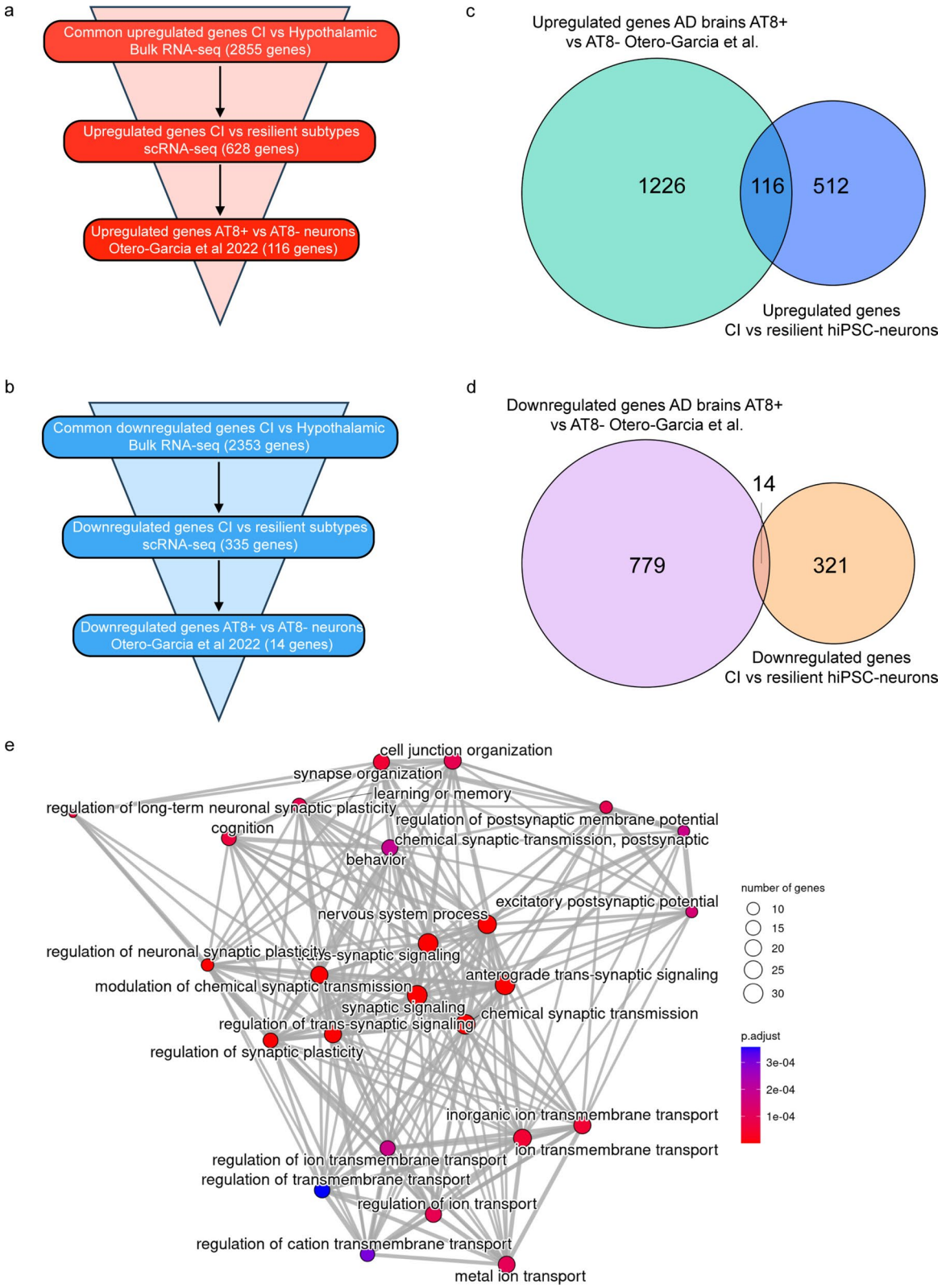

Fig. 6 (See legend on previous page.)

and regulation of membrane potential. Differentially expressed genes contributing to these pathways included numerous gamma-aminobutyric acid (GABA) receptor subunit genes (*GABRA1*, *GABRA4*, *GABRA5*, *GABRB2*), solute carrier family members involved in presynaptic uptake of neurotransmitters (*SLC6 A17*) and sodium-calcium exchange (*SLC24 A2*), and the N-methyl-D-aspartate (NMDA) receptor subunit, *GRIN2B* (Additional File 6). *GABRA1* and *GRIN2B* upregulation in NFT-bearing neurons was histologically validated by Otero-Garcia et al., confirming the link between AD Tau aggregation and increased expression of these genes [64]. These findings derived from bulk and single cell RNA-seq analysis of baseline transcriptional differences between the Tau-vulnerable cortical inhibitory hiPSC-neurons and the Tau-resilient hypothalamic hiPSC-neurons highlight processes relevant to Tau propagation [19, 25, 87] and are consistent with data derived from AD patient neurons [64], supporting the disease relevance of the hiPSC-neuron seeding model and its ability to recapitulate selective vulnerability, a key feature of AD and other late-onset neurodegenerative diseases.

Discussion

Recently, numerous studies in AD brain tissue have highlighted the selective vulnerability of specific neuronal subtypes to Tau pathology [17, 32, 46, 54, 62]; however, model systems which recapitulate features of selective vulnerability are lacking. While some studies with patient-derived lines have observed phenotypes compared to apparently healthy donor controls [9, 60, 61], the phenotypes are often mild and/or inconsistent which is likely in part due to the age of the hiPSC-neurons which does not align with the late-onset nature of neurodegenerative disease [80]. This challenge has been partially overcome by using protein aggregate seeding to initiate the protein pathology characteristic of many neurodegenerative diseases. Along these lines, a prior study in hiPSC-neurons derived from carriers of familial AD (fAD) associated amyloid precursor protein (APP) mutations showed increased production of Aβ in addition to increased Tau phosphorylation at serine 202 and elevated total Tau protein levels in rostral hiPSC-neurons relative to caudal hiPSC-neurons in response to exogenous Aβ aggregates [60, 61]. This study demonstrated the capacity for hiPSC models to exhibit features that may be associated with familial AD in a cell type-specific manner via seeding. However, the question remained whether Tau aggregation, which more closely correlates with cognitive decline in AD [6, 53], would also follow a pattern of susceptibility that aligns with the human disease in undiagnosed, apparently healthy hiPSC-derived neurons in the absence of other neural cell types and irrespective of genetic background.

To test this hypothesis, we took advantage of our recently established human in vitro model of endogenous Tau aggregation via seeding using AD patient-derived pathological Tau in hiPSC-derived neuronal cultures [51]. In our analysis of seeded Tau aggregation in 5 distinct hiPSC-neuron subtypes, CTIP2-positive, SST-positive cortical inhibitory hiPSC-neurons displayed the highest relative vulnerability to Tau pathology among the subtypes evaluated. Similarly, a recent report highlighted three vulnerable classes of SST-positive cortical inhibitory neurons in AD patients [54]. The study measured, via single-nucleus RNA-seq (snRNA-seq), the relative abundance of neuronal subtypes in individuals with different levels of AD pathology, finding that SST-positive cortical inhibitory neurons were preferentially lost in individuals with high pathology burden [54]. While differences between hiPSC-derived neuronal subtypes were defined by their Tau aggregation load rather than neuronal loss in our study, our data suggests that Tau aggregation follows a similar pattern of accumulation, supporting the disease relevance of the in vitro model system.

Remarkably, we observed consistency in the pattern of susceptibility across different Tau aggregate preparations utilized to template the endogenous Tau. While SS-AD is structurally distinct from mature PHF [40], SS-AD not only induced aggregation in hiPSC-neurons in line with a recent publication demonstrating that PBS-extracted Tau aggregates from AD patient brain tissue are capable of propagating Tau pathology [40], but the exogenous seed preparation also showed highest aggregation levels in cortical inhibitory neurons similar to SI-AD. The pattern of susceptibility triggered by both fractions indicates that common mechanisms may govern the Tau propagation induced by a variety of pathological species.

While we observed distinct uptake rates and an increased rate of Tau degradation between neuronal subtypes, they did not correlate with Tau aggregation levels and therefore resilience. Uptake and degradation experiments relied on recombinant Tau aggregates, which is not a stimulator of endogenous Tau aggregation in hiPSC-neurons lacking Tau mutations [51]. Therefore, they could follow different uptake pathways than human-derived Tau aggregates and be the source of disconnect between recombinant Tau aggregate uptake rates and aggregation levels triggered by SI-AD material. We addressed this possibility through a SI-AD transfection experiment. The results suggested that avoiding endogenous Tau-aggregate uptake pathways by using transfection agents significantly increased Tau aggregation regardless of neuronal subtype. Taken together, these data indicate that Tau aggregate uptake and degradation

mechanisms may be rate limiting but are not sufficient to explain differential vulnerability to Tau pathology among the 5 hiPSC-derived neuronal subtypes.

Digging further into endosomal trafficking, we found that RAB7 A knockdown increased Tau aggregation irrespective of hiPSC-neuron subtype. This finding suggests altered vesicle trafficking modulates seeding induced Tau aggregation in our model system but does not implicate RAB7 A in selective vulnerability. However, there are numerous Rab proteins contributing to vesicle trafficking beyond RAB7 A and future studies on vesicle transport's role in selective vulnerability could clarify the mechanistic basis for subtype-specific patterns of aggregation.

To broaden our hiPSC-neuron model of selective vulnerability via seeding beyond Tau, we showed that our model can also distinguish the disease-specific vulnerability between different protein aggregates. Following seeding with α-synuclein PFFs, mDA hiPSC-neurons displayed higher levels of pS129 α-synuclein aggregates relative to cortical hiPSC-neurons as observed in Parkinson's Disease patients where first dopaminergic neurons succumb to α-synuclein pathology whereas cortical neurons are affected much later or not at all [16, 76]. These observations which mirror susceptibility in patients shows that carefully patterned hiPSC-neurons are capable of recapitulating aspects of selective vulnerability across neurodegenerative diseases.

Surprisingly, we did not observe a consistent transcriptional response to aggregate seeding in hiPSC-neurons that could shed light on the molecular underpinnings of neuronal resilience. Given that scRNA-seq revealed some heterogeneity within each subtype/protocol as represented by a few transcriptomically distinct clusters and that aggregates do not appear in every neuron within the timeframe of the assay, transcriptional responses could be masked by pooling cells together. Therefore, techniques which measure changes specific to aggregate-bearing neurons could assist future studies in identifying potential gene and protein changes triggered by the presence of aggregates, similar to the work from Otero-Garcia et al. [64]. Narrowing in on the neurons with the most Tau pathology using single cell resolution techniques such as spatial transcriptomics could further our understanding of selective vulnerability and increase our chances of identifying mediators of this process.

Nevertheless, selective vulnerability mediators might be identified from the baseline transcriptional differences between vulnerable and resilient hiPSC-neurons. Because the hypothalamic hiPSC-neurons were derived from the same NPCs as the highly vulnerable cortical inhibitory neurons and express several overlapping marker genes (*FOXG1*, *SST*, *SLC32 A1*), we took advantage of their closer lineage relationship to define a transcriptomic signature of differentially expressed genes between these neuronal subtypes. We reasoned that the comparison of two forebrain neuronal subtypes would be more likely to uncover expression patterns underlying selective vulnerability than comparing forebrain versus mid/hindbrain neurons due to their greater similarity yet drastic differences in propensity to form Tau aggregates. The differentially expressed genes (DEGs) between Tau-vulnerable cortical inhibitory hiPSC-neurons and Tau-resilient hypothalamic hiPSC-neurons were enriched for genes related to ion transport and synapse homeostasis. Evidence for a potential connection between synaptic function and Tau pathology includes the hypothesized spread of Tau between synaptically-connected neurons [18, 19, 25, 58] and the dependence of spreading on neuronal/synaptic activity, which might be a contributing factor in our experimental system [66, 68, 87]. Beyond synaptic DEGs, transcriptional changes associated with calcium homeostasis were also highlighted by enrichment analyses of upregulated genes in cortical inhibitory hiPSC-neurons compared to hypothalamic hiPSC-neurons. Associations between calcium homeostasis and Tau aggregates have been described in NFT-bearing neurons relative to NFT-free AD neurons where altered gene expression of calcium homeostasis pathways have been found. Furthermore, the function of numerous Tau kinases and phosphatases are dependent on calcium, as is calpain-mediated Tau cleavage [11, 23, 34, 41, 43], and therefore might contribute to the selective vulnerability. Future experiments utilizing genetic knockdown or knockout will be needed to systematically determine the contribution of these differentially expressed genes to the observed susceptibility to Tau aggregate formation.

To determine whether the observed differences in gene expression between Tau-vulnerable and Tau-resilient hiPSC-neurons were relevant to Tau aggregation in the disease, differentially expressed genes in Tau-vulnerable hiPSC-neurons were compared to the gene expression changes found by Otero-Garcia et al. in AT8-positive versus AT8-negative neurons derived from AD patient brains. This analysis revealed a strong enrichment of genes related to synaptic function and membrane potential. The study by Otero-Garcia et al. observed altered synaptic gene expression to be a common feature of NFT-bearing AD neurons, regardless of cell identity [64]. These findings raise the question as to whether synaptic gene expression changes are a cause or consequence of AD pathology. Determining whether altered expression of synaptic genes enhances vulnerability to Tau pathology in hiPSC-neurons is beyond the scope of this study but represents an exciting avenue for future exploration.

Conclusions

Our initial characterization shows that uptake and proteostatic mechanisms do not fully explain the observed vulnerabilities, which now opens the opportunity to systematically validate the role of differentially expressed neuron-subclass-specific genes in governing susceptibility in future studies. Importantly, the human neuron model system proposed here makes this possible using disease-relevant neurons and exogenous seeds to induce endogenous aggregation, increasing the likelihood of translation to human disease. Application of this platform to uncover genes or whole pathways conferring vulnerability or resistance in vitro represents an exciting new approach to aid in developing therapeutics that could slow disease progression or even prevent neurodegeneration.

Abbreviations

AD	Alzheimer's disease
DIV	Days in vitro after final replating of neuron-committed population across all protocols
fAD	Familial Alzheimer's disease
hiPSC	Human induced pluripotent stem cells
MC1-AD	AD brain-derived protein immunopurified with MC1 antibody
mDA	Midbrain dopaminergic
NFT	Neurofibrillary tangle
NTC	Non-targeting control
PD	Parkinson's disease
PFF	Pre-formed fibril
qRT-PCR/qPCR	Quantitative rela-time polymerase chain reaction
RORB	RAR related orphan receptor B
scRNA-seq	Single cell RNA sequencing
SI-AD	Sarkosyl insoluble AD brain-derived protein
SNP	Single nucleotide polymorphism
snRNA-seq	Single nuclei RNA sequencing
sPHF	Sonicated paired helical filaments
SS-AD	Sarkosyl soluble AD brain-derived protein
SST	Somatostatin

Supplementary Information

The online version contains supplementary material available at https://doi.org/10.1186/s40478-025-02000-4.

Additional File 1.

Upregulated and downregulated genes in cortical inhibitory hiPSC-neurons. Excel.xlsx. List of genes commonly differentially expressed across 3 hiPSC donor lines from bulk RNA-seq comparison of cortical inhibitory versus hypothalamic hiPSC-neurons

Additional File 2.

Pathway enrichment of upregulated genes in cortical inhibitory hiPSC-neurons. Excel.xls. Complete pathway enrichment results from the 2,855 common upregulated genes in cortical inhibitory hiPSC-neurons vs hypothalamic hiPSC-neurons across three hiPSC donor lines identified via bulk RNA-seq

Additional File 3.

Pathway enrichment of downregulated genes in cortical inhibitory hiPSC-neurons. Excel.xls. Complete pathway enrichment results from the 2,353 common downregulated genes in cortical hiPSC-neurons vs hypothalamic hiPSC-neurons across three hiPSC donor lines identified via bulk RNA-seq

Additional File 4.

Commonly upregulated genes in cortical inhibitory hiPSC-neurons and NFT-bearing neurons. Excel.xls. List of genes upregulated in cortical inhibitory hiPSC-neurons vs hypothalamic hiPSC-neurons and in AT8-positive vs AT8-negative neurons from Otero-Garcia et al. [64]

Additional File 5.

Commonly downregulated genes in cortical inhibitory hiPSC-neurons and NFT-bearing neurons. Excel.xls. List of genes downregulated in cortical inhibitory hiPSC-neurons vs hypothalamic hiPSC-neurons and in AT8-positive vs AT8-negative neurons from Otero-Garcia et al. [64]

Additional File 6.

Pathway enrichment of cortical inhibitory hiPSC-neuron upregulated genes shared with AT8-positive neurons from AD brains. Excel.xls. Complete pathway enrichment results from the overlapping upregulated genes between our vulnerable cortical inhibitory hiPSC-neurons relative to resilient hiPSC-neurons and AT8-positive vs AT8-negative neurons from Otero-Garcia et al. [64]

Additional File 7.

Supplementary Figures 1-11

Acknowledgements

We would like to thank the Massachusetts Alzheimer's Disease Research Center for donated AD and non-AD brain tissue. Special thanks to Peter Davies of Feinstein Institute for providing PHF1 and MC1 antibodies. These reagents were received through a Material Transfer Agreement. Images in Fig. 1a, Fig. 3a, and Fig. 5a were created with BioRender.com. Visualizations of single cell-RNA-seq data in Supp. Fig. 2, Fig. 4a and Supp. Fig. 11b were performed using Bioturing's BBrowser tool. Financial support for this research was provided by AbbVie.

Author contributions

I.W., C.N.P., S.E.C., L.G., G.L., M.S.B., J.L., L.M.R., O.M., K.N.N., N.R.P., G.S., M.W., Q.L., P.R., R.W., D.E.E., A.S., S.B., C.X., B.S., M.C., N.R., K.Y., A.M.W., J.W., L.G., J.S., X.L., T.J.K. and J.D.M contributed to the study conception and design. Material preparation, data collection, and analysis were performed by I.W., C.N.P., S.E.C., L.G., G.L., M.S.B., J.L., L.M.R., O.M., K.N.N., N.R.P., Q.L., P.R., R.W., D.E.E., A.S., S.B., C.X., B.S., M.C., N.R., K.Y., J.W., T.J.K., and J.D.M. The first draft of the manuscript was written by I.W. and J.D.M. and all authors commented on previous versions of the manuscript. All authors read and approved the final manuscript.

Funding

The design, study conduct, and financial support for this research were provided by AbbVie.

Availability of data and material

The bulk RNA-seq data in FASTQ format has been deposited in the NCBI short read archive (SRA), accession PRJNA1139100. The processed single cell RNA-seq data has been uploaded to zenodo.org (doi https://doi.org/10.5281/zenodo.14873475).

Declarations

Ethics approval and consent to participate

Written informed consent for primary tissue procurement and the use of the material and clinical information for research purposes was obtained by the brain banks and the hiPSC providers (commercial sources or consortiums) used in this study.

Consent for publication

Not applicable.

Competing interests

Funding/Competing interests C.N.P., S.E.C., L.G., G.L., M.S.B., J.L., L.M.R., O.M., K.N.N., N.R.P., Q.L., P.R., R.W., D.E.E., A.S., S.B., C.X., B.S., M.C., N.R., K.Y., A.M.W., J.W.,

L.G., J.S., X.L., and J.D.M are employees of AbbVie. I.W., G.S. T.J.K, and M.W. were employees at the time of the study. The design, study conduct, and financial support for this research were provided by AbbVie. AbbVie participated in the interpretation of data, review, and approval of the publication.

Author details
[1]AbbVie, Cambridge Research Center, 200 Sidney Street, Cambridge, MA 02139, USA. [2]AbbVie Pte Ltd, 9 North Buona Vista Drive #19-01, Singapore 138588, Singapore. [3]AbbVie, Chicago, USA. [4]AbbVie Deutschland GmbH & Co. KG, 67061 Ludwigshafen, Germany.

Received: 27 September 2024 Accepted: 5 April 2025
Published online: 19 May 2025

References

1. Aleksander SA, Balhoff J, Carbon S, Cherry JM, Drabkin HJ, Ebert D, Feuermann M, Gaudet P, Harris NL, Hill DP, Lee R, Mi H, Moxon S, Mungall CJ, Muruganugan A, Mushayahama T, Sternberg PW, Thomas PD, Auken KV, Ramsey J, Siegele DA, Chisholm RL, Fey P, Aspromonte MC, Nugnes MV, Quaglia F, Tosatto S, Giglio M, Nadendla S, Antonazzo G, Attrill H, dos Santos G, Marygold S, Strelets V, Tabone CJ, Thurmond J, Zhou P, Ahmed SH, Asanitthong P, Buitrago DL, Erdol MN, Gage MC, Kadhum MA, Li KYC, Long M, Michalak A, Pesala A, Pritazahra A, Saverimuttu SCC, Su R, Thurlow KE, Lovering RC, Logie C, Oliferenko S, Blake J, Christie K, Corbani L, Dolan ME, Drabkin HJ, Hill DP, Ni L, Sitnikov D, Smith C, Cuzick A, Seager J, Cooper L, Elser J, Jaiswal P, Gupta P, Jaiswal P, Naithani S, Lera-Ramirez M, Rutherford K, Wood V, Pons JLD, Dwinell MR, Hayman GT, Kaldunski ML, Kwitek AE, Laulederkind SJF, Tutaj MA, Vedi M, Wang S-J, D'Eustachio P, Aimo L, Axelsen K, Bridge A, Hyka-Nouspikel N, Morgat A, Aleksander SA, Cherry JM, Engel SR, Karra K, Miyasato SR, Nash RS, Skrzypek MS, Weng S, Wong ED, Bakker E, Berardini TZ, Reiser L, Auchincloss A, Axelsen K, Argoud-Puy G, Blatter M-C, Boutet E, Breuza L, Bridge A, Casals-Casas C, Coudert E, Estreicher A, Famiglietti ML, Feuermann M, Gos A, Gruaz-Gumowski N, Hulo C, Hyka-Nouspikel N, Jungo F, Mercier PL, Lieberherr D, Masson P, Morgat A, Pedruzzi I, Pourcel L, Poux S, Rivoire C, Sundaram S, Bateman A, Bowler-Barnett E, Bye-A-Jee H, Denny P, Ignatchenko A, Ishtiaq R, Lock A, Lussi Y, Magrane M, Martin MJ, Orchard S, Raposo P, Speretta E, Tyagi N, Warner K, Zaru R, Diehl AD, Lee R, Chan J, Diamantakis S, Raciti D, Zarowiecki M, Fisher M, James-Zorn C, Ponferrada V, Zorn A, Ramachandran S, Ruzicka L, Westerfield M, Aleksander SA, Balhoff J, Carbon S, Cherry JM, Drabkin HJ, Ebert D, Feuermann M, Gaudet P, Harris NL, Hill DP, Lee R, Mi H, Moxon S, Mungall CJ, Muruganugan A, Mushayahama T, Sternberg PW, Thomas PD, Auken KV, Ramsey J, Siegele DA, Chisholm RL, Fey P, Aspromonte MC, Nugnes MV, Quaglia F, Tosatto S, Giglio M, Nadendla S, Antonazzo G, Attrill H, dos Santos G, Marygold S, Strelets V, Tabone CJ, Thurmond J, Zhou P, Ahmed SH, Asanitthong P, Buitrago DL, Erdol MN, Gage MC, Kadhum MA, Li KYC, Long M, Michalak A, Pesala A, Pritazahra A, Saverimuttu SCC, Su R, Thurlow KE, Lovering RC, Logie C, Oliferenko S, Blake J, Christie K, Corbani L, Dolan ME, Drabkin HJ, Hill DP, Ni L, Sitnikov D, Smith C, Cuzick A, Seager J, Cooper L, Elser J, Jaiswal P, Gupta P, Jaiswal P, Naithani S, Lera-Ramirez M, Rutherford K, Wood V, Pons JLD, Dwinell MR, Hayman GT, Kaldunski ML, Kwitek AE, Laulederkind SJF, Tutaj MA, Vedi M, Wang S-J, D'Eustachio P, Aimo L, Axelsen K, Bridge A, Hyka-Nouspikel N, Morgat A, Aleksander SA, Cherry JM, Engel SR, Karra K, Miyasato SR, Nash RS, Skrzypek MS, Weng S, Wong ED, Bakker E, Berardini TZ, Reiser L, Auchincloss A, Axelsen K, Argoud-Puy G, Blatter M-C, Boutet E, Breuza L, Bridge A, Casals-Casas C, Coudert E, Estreicher A, Famiglietti ML, Feuermann M, Gos A, Gruaz-Gumowski N, Hulo C, Hyka-Nouspikel N, Jungo F, Mercier PL, Lieberherr D, Masson P, Morgat A, Pedruzzi I, Pourcel L, Poux S, Rivoire C, Sundaram S, Bateman A, Bowler-Barnett E, Bye-A-Jee H, Denny P, Ignatchenko A, Ishtiaq R, Lock A, Lussi Y, Magrane M, Martin MJ, Orchard S, Raposo P, Speretta E, Tyagi N, Warner K, Zaru R, Diehl AD, Lee R, Chan J, Diamantakis S, Raciti D, Zarowiecki M, Fisher M, James-Zorn C, Ponferrada V, Zorn A, Ramachandran S, Ruzicka L, Westerfield M (2023) The Gene ontology knowledgebase in 2023. Genetics 224:iyad031. https://doi.org/10.1093/genetics/iyad031
2. Ashburner M, Ball CA, Blake JA, Botstein D, Butler H, Cherry JM, Davis AP, Dolinski K, Dwight SS, Eppig JT, Harris MA, Hill DP, Issel-Tarver L, Kasarskis A, Lewis S, Matese JC, Richardson JE, Ringwald M, Rubin GM, Sherlock G (2000) Gene Ontology: tool for the unification of biology. Nat Genet 25:25–29. https://doi.org/10.1038/75556
3. Barini E, Plotzky G, Mordashova Y, Hoppe J, Rodriguez-Correa E, Julier S, LePrieult F, Mairhofer I, Mezler M, Biesinger S, Cik M, Meinhardt MW, Ercan-Herbst E, Ehrnhoefer DE, Striebinger A, Bodie K, Klein C, Gasparini L, Schlegel K (2022) Tau in the brain interstitial fluid is fragmented and seeding–competent. Neurobiol Aging 109:64–77. https://doi.org/10.1016/j.neurobiolaging.2021.09.013
4. Bichmann M, Oriol NP, Ercan-Herbst E, Schöndorf DC, Ramos BG, Schwärzler V, Neu M, Schlüter A, Wang X, Jin L, Hu C, Tian Y, Ried JS, Haberkant P, Gasparini L, Ehrnhoefer DE (2021) SETD7-mediated monomethylation is enriched on soluble Tau in Alzheimer's disease. Mol Neurodegener 16:46. https://doi.org/10.1186/s13024-021-00468-x
5. Blum H, Beier H, Gross HJ (1987) Improved silver staining of plant proteins, RNA and DNA in polyacrylamide gels. Electrophoresis 8:93–99. https://doi.org/10.1002/elps.1150080203
6. Braak H, Braak E (1991) Neuropathological stageing of Alzheimer-related changes. Acta Neuropathol 82:239–259. https://doi.org/10.1007/bf00308809
7. Braak H, Braak E, Bohl J (1993) Staging of Alzheimer-related cortical destruction. Eur Neurol 33:403–408. https://doi.org/10.1159/000116984
8. Braak H, del Tredici K, Schultz C, Braak EVA (2000) Vulnerability of select neuronal types to alzheimer's disease. Ann New York Acad Sci 924(1):53–61. https://doi.org/10.1111/j.1749-6632.2000.tb05560.x
9. Brazdis R-M, Alecu J, Marsch D, Dahms A, Simmnacher K, Lörentz S, Brendler A, Schneider Y, Marxreiter F, Roybon L, Winner B, Xiang W, Prots I (2020) Demonstration of brain region-specific neuronal vulnerability in human iPSC-based model of familial Parkinson's disease. Hum Mol Genet 29:1180–1191. https://doi.org/10.1093/hmg/ddaa039
10. Calafate S, Buist A, Miskiewicz K, Vijayan V, Daneels G, de Strooper B, de Wit J, Verstreken P, Moechars D (2015) Synaptic contacts enhance cell-to-cell tau pathology propagation. Cell Rep 11:1176–1183. https://doi.org/10.1016/j.celrep.2015.04.043
11. Cao L-L, Guan P-P, Liang Y-Y, Huang X-S, Wang P (2019) Calcium Ions stimulate the hyperphosphorylation of Tau by activating microsomal prostaglandin E synthase 1. Front Aging Neurosci 11:108. https://doi.org/10.3389/fnagi.2019.00108
12. Chambers SM, Fasano CA, Papapetrou EP, Tomishima M, Sadelain M, Studer L (2009) Highly efficient neural conversion of human ES and iPS cells by dual inhibition of SMAD signaling. Nat Biotechnol 27:275–280. https://doi.org/10.1038/nbt.1529
13. Chen JJ, Nathaniel DL, Raghavan P, Nelson M, Tian R, Tse E, Hong JY, See SK, Mok S-A, Hein MY, Southworth DR, Grinberg LT, Gestwicki JE, Leonetti MD, Kampmann M (2019) Compromised function of the ESCRT pathway promotes endolysosomal escape of tau seeds and propagation of tau aggregation. J Biol Chem 294:18952–18966. https://doi.org/10.1074/jbc.ra119.009432
14. Chmielarz P, Domanskyi A (2021) Alpha-synuclein preformed fibrils: a tool to understand Parkinson's disease and develop disease modifying therapy. Neural Regen Res 16:2219–2221. https://doi.org/10.4103/1673-5374.310686
15. Cicognola C, Brinkmalm G, Wahlgren J, Portelius E, Gobom J, Cullen NC, Hansson O, Parnetti L, Constantinescu R, Wildsmith K, Chen H-H, Beach TG, Lashley T, Zetterberg H, Blennow K, Höglund K (2019) Novel tau fragments in cerebrospinal fluid: relation to tangle pathology and cognitive decline in Alzheimer's disease. Acta Neuropathol 137:279–296. https://doi.org/10.1007/s00401-018-1948-2
16. Damier P, Hirsch EC, Agid Y, Graybiel AM (1999) The substantia nigra of the human brainII. Patterns of loss of dopamine-containing neurons in Parkinson's disease. Brain 122:1437–1448. https://doi.org/10.1093/brain/122.8.1437
17. Davila-Velderrain J, Mathys H, Mohammadi S, Ruzicka B, Jiang X, Ng A, Bennett DA, Tsai L-H, Kellis M (2021) Single-cell anatomical analysis of human hippocampus and entorhinal cortex uncovers early-stage molecular pathology in Alzheimer's disease. bioRxiv 2021.07.01.450715
18. de Calignon A, Polydoro M, Suárez-Calvet M, William C, Adamowicz DH, Kopeikina KJ, Pitstick R, Sahara N, Ashe KH, Carlson GA, Spires-Jones TL, Hyman BT (2012) Propagation of Tau pathology in a model of early alzheimer's disease. Neuron 73:685–697. https://doi.org/10.1016/j.neuron.2011.11.033

19. DeVos SL, Corjuc BT, Oakley DH, Nobuhara CK, Bannon RN, Chase A, Commins C, Gonzalez JA, Dooley PM, Frosch MP, Hyman BT (2018) Synaptic Tau seeding precedes Tau pathology in human alzheimer's disease brain. Front Neurosci 12:267. https://doi.org/10.3389/fnins.2018.00267
20. Dobin A, Davis CA, Schlesinger F, Drenkow J, Zaleski C, Jha S, Batut P, Chaisson M, Gingeras TR (2013) STAR: ultrafast universal RNA-seq aligner. Bioinformatics 29:15–21. https://doi.org/10.1093/bioinformatics/bts635
21. Du Z-W, Chen H, Liu H, Lu J, Qian K, Huang C-L, Zhong X, Fan F, Zhang S-C (2015) Generation and expansion of highly pure motor neuron progenitors from human pluripotent stem cells. Nat Commun 6:6626. https://doi.org/10.1038/ncomms7626
22. Evans LD, Wassmer T, Fraser G, Smith J, Perkinton M, Billinton A, Livesey FJ (2018) Extracellular monomeric and aggregated Tau efficiently enter human neurons through overlapping but distinct pathways. Cell Rep 22:3612–3624. https://doi.org/10.1016/j.celrep.2018.03.021
23. Ferreira A, Bigio EH (2011) Calpain-Mediated Tau cleavage: A mechanism leading to neurodegeneration shared by multiple tauopathies. Mol Med 17:676–685. https://doi.org/10.2119/molmed.2010.00220
24. Forsell C, Björk BF, Lilius L, Axelman K, Fabre SF, Fratiglioni L, Winblad B, Graff C (2010) Genetic association to the amyloid plaque associated protein gene COL25A1 in Alzheimer's disease. Neurobiol Aging 31:409–415. https://doi.org/10.1016/j.neurobiolaging.2008.04.009
25. Frost B, Jacks RL, Diamond MI (2009) Propagation of Tau misfolding from the outside to the inside of a cell*. J Biol Chem 284:12845–12852. https://doi.org/10.1074/jbc.m808759200
26. Fu H, Hardy J, Duff KE (2018) Selective vulnerability in neurodegenerative diseases. Nat Neurosci 21:1350–1358. https://doi.org/10.1038/s41593-018-0221-2
27. Fujiwara H, Hasegawa M, Dohmae N, Kawashima A, Masliah E, Goldberg MS, Shen J, Takio K, Iwatsubo T (2002) α-synuclein is phosphorylated in synucleinopathy lesions. Nat Cell Biol 4:160–164. https://doi.org/10.1038/ncb748
28. Gerando AMD, Welikovitch LA, Khasnavis A, Commins C, Glynn C, Chun JE, Perbet R, Hyman BT (2023) Tau seeding and spreading in vivo is supported by both AD-derived fibrillar and oligomeric tau. Acta Neuropathol 146:191–210. https://doi.org/10.1007/s00401-023-02600-1
29. Germain P-L, Lun A, Meixide CG, Macnair W, Robinson MD (2021) Doublet identification in single-cell sequencing data using scDblFinder. F1000Research 10:979. https://doi.org/10.12688/f1000research.73600.2
30. Goedert M, Spillantini MG (2017) Propagation of Tau aggregates. Mol. Brain 10:18. https://doi.org/10.1186/s13041-017-0298-7
31. González-Hernández T, Cruz-Muros I, Afonso-Oramas D, Salas-Hernandez J, Castro-Hernandez J (2010) Vulnerability of mesostriatal dopaminergic neurons in parkinson's disease. Front Neuroanat 4:140. https://doi.org/10.3389/fnana.2010.00140
32. Grubman A, Choo XY, Chew G, Ouyang JF, Sun G, Croft NP, Rossello FJ, Simmons R, Buckberry S, Landin DV, Pflueger J, Vandekolk TH, Abay Z, Zhou Y, Liu X, Chen J, Larcombe M, Haynes JM, McLean C, Williams S, Chai SY, Wilson T, Lister R, Pouton CW, Purcell AW, Rackham OJL, Petretto E, Polo JM (2021) Transcriptional signature in microglia associated with Aβ plaque phagocytosis. Nat Commun 12:3015. https://doi.org/10.1038/s41467-021-23111-1
33. Hao Y, Hao S, Andersen-Nissen E, Mauck WM, Zheng S, Butler A, Lee MJ, Wilk AJ, Darby C, Zagar M, Hoffman P, Stoeckius M, Papalexi E, Mimitou EP, Jain J, Srivastava A, Stuart T, Fleming LB, Yeung B, Rogers AJ, McElrath JM, Blish CA, Gottardo R, Smibert P, Satija R (2020) Integrated analysis of multimodal single-cell data. bioRxiv 2020.10.12.335331
34. Hartigan JA, Johnson GVW (1999) Transient Increases in intracellular calcium result in prolonged site-selective increases in Tau phosphorylation through a glycogen synthase kinase 3β-dependent pathway*. J Biol Chem 274:21395–21401. https://doi.org/10.1074/jbc.274.30.21395
35. Hashimoto T, Wakabayashi T, Watanabe A, Kowa H, Hosoda R, Nakamura A, Kanazawa I, Arai T, Takio K, Mann DMA, Iwatsubo T (2002) CLAC: a novel Alzheimer amyloid plaque component derived from a transmembrane precursor, CLAC-P/collagen type XXV. EMBO J 21:1524–1534. https://doi.org/10.1093/emboj/21.7.1524
36. He Z, Yu Q (2018) Identification and characterization of functional modules reflecting transcriptome transition during human neuron maturation. BMC Genom 19:262. https://doi.org/10.1186/s12864-018-4649-2
37. Holmes BB, Furman JL, Mahan TE, Yamasaki TR, Mirbaha H, Eades WC, Belaygorod L, Cairns NJ, Holtzman DM, Diamond MI (2014) Proteopathic tau seeding predicts tauopathy in vivo. Proc Natl Acad Sci 111:E4376–E4385. https://doi.org/10.1073/pnas.1411649111
38. Hyttinen JMT, Niittykoski M, Salminen A, Kaarniranta K (2013) Maturation of autophagosomes and endosomes: a key role for Rab7. Biochim Biophy Acta (BBA) - Mol Cell Res 1833:503–510. https://doi.org/10.1016/j.bbamcr.2012.11.018
39. Jackson SJ, Kerridge C, Cooper J, Cavallini A, Falcon B, Cella CV, Landi A, Szekeres PG, Murray TK, Ahmed Z, Goedert M, Hutton M, O'Neill MJ, Bose S (2016) Short fibrils constitute the major species of seed-competent Tau in the brains of mice transgenic for human P301S Tau. J Neurosci 36:762–772. https://doi.org/10.1523/jneurosci.3542-15.2016
40. Jicha GA, Bowser R, Kazam IG, Davies P (1997) Alz-50 and MC-1, a new monoclonal antibody raised to paired helical filaments, recognize conformational epitopes on recombinant tau. J Neurosci Res 48:128–132. https://doi.org/10.1002/(sici)1097-4547(19970415)48:2%3c128::aid-jnr5%3e3.0.co;2-e
41. Johnson GVW, Jope RS, Binder LI (1989) Proteolysis of tau by calpain. Biochem Biophys Res Commun 163:1505–1511. https://doi.org/10.1016/0006-291x(89)91150-9
42. Meredith JE Jr, Sankaranarayanan S, Guss V, Lanzetti AJ, Berisha F, Neely RJ, Albright CF (2013) Characterization of novel CSF Tau and ptau biomarkers for alzheimer's disease. PLoS ONE 8:e76523. https://doi.org/10.1371/journal.pone.0076523
43. Karch CM, Jeng AT, Goate AM (2013) Calcium phosphatase calcineurin influences tau metabolism. Neurobiol Aging 34:374–386. https://doi.org/10.1016/j.neurobiolaging.2012.05.003
44. Koopmans F, van Nierop P, Andres-Alonso M, Byrnes A, Cijsouw T, Coba MP, Cornelisse LN, Farrell RJ, Goldschmidt HL, Howrigan DP, Hussain NK, Imig C, de Jong APH, Jung H, Kohansalnodehi M, Kramarz B, Lipstein N, Lovering RC, MacGillavry H, Mariano V, Mi H, Ninov M, Osumi-Sutherland D, Pielot R, Smalla K-H, Tang H, Tashman K, Toonen RFG, Verpelli C, Reig-Viader R, Watanabe K, van Weering J, Achsel T, Ashrafi G, Asi N, Brown TC, Camilli PD, Feuermann M, Foulger RE, Gaudet P, Joglekar A, Kanellopoulos A, Malenka R, Nicoll RA, Pulido C, de Juan-Sanz J, Sheng M, Südhof TC, Tilgner HU, Bagni C, Bayés À, Biederer T, Brose N, Chua JJE, Dieterich DC, Gundelfinger ED, Hoogenraad C, Huganir RL, Jahn R, Kaeser PS, Kim E, Kreutz MR, McPherson PS, Neale BM, O'Connor V, Posthuma D, Ryan TA, Sala C, Feng G, Hyman SE, Thomas PD, Smit AB, Verhage M (2019) SynGO: an evidence-based, expert-curated knowledge base for the synapse. Neuron 103:217-234.e4. https://doi.org/10.1016/j.neuron.2019.05.002
45. Kumar M, Quittot N, Dujardin S, Schlaffner CN, Viode A, Wiedmer A, Beerepoot P, Chun JE, Glynn C, Fernandes AR, Donahue C, Steen JA, Hyman BT (2024) Alzheimer proteopathic tau seeds are biochemically a forme fruste of mature paired helical filaments. Brain 147:637–648. https://doi.org/10.1093/brain/awad378
46. Leng K, Li E, Eser R, Piergies A, Sit R, Tan M, Neff N, Li SH, Rodriguez RD, Suemoto CK, Leite REP, Ehrenberg AJ, Pasqualucci CA, Seeley WW, Spina S, Heinsen H, Grinberg LT, Kampmann M (2021) Molecular characterization of selectively vulnerable neurons in Alzheimer's disease. Nat Neurosci 24:276–287. https://doi.org/10.1038/s41593-020-00764-7
47. Liao Y, Smyth GK, Shi W (2013) featureCounts: An efficient general-purpose program for assigning sequence reads to genomic features
48. Limorenko G, Tatli M, Kolla R, Nazarov S, Weil M-T, Schöndorf DC, Geist D, Reinhardt P, Ehrnhoefer DE, Stahlberg H, Gasparini L, Lashuel HA (2023) Fully co-factor-free CLEARTAU platform produces seeding-competent Tau fibrils for reconstructing pathological Tau aggregates. Nat Commun 14:3939. https://doi.org/10.1038/s41467-023-39314-7
49. Liu H, Zhang S-C (2011) Specification of neuronal and glial subtypes from human pluripotent stem cells. Cell Mol Life Sci 68:3995–4008. https://doi.org/10.1007/s00018-011-0770-y
50. Love MI, Huber W, Anders S (2014) Moderated estimation of fold change and dispersion for RNA-seq data with DESeq2. Genome Biol 15:550. https://doi.org/10.1186/s13059-014-0550-8
51. Manos JD, Preiss CN, Venkat N, Tamm J, Reinhardt P, Kwon T, Wu J, Winter AD, Jahn TR, Yanamandra K, Titterton K, Karran E, Langlois X (2022) Uncovering specificity of endogenous TAU aggregation in a human iPSC-neuron TAU seeding model. iScience 25:103658. https://doi.org/10.1016/j.isci.2021.103658
52. Martin M (2011) Cutadapt removes adapter sequences from high-throughput sequencing reads. EMBnetJ 17:10–12. https://doi.org/10.14806/ej.17.1.200

53. Mathys H, Davila-Velderrain J, Peng Z, Gao F, Mohammadi S, Young JZ, Menon M, He L, Abdurrob F, Jiang X, Martorell AJ, Ransohoff RM, Hafler BP, Bennett DA, Kellis M, Tsai L-H (2019) Single-cell transcriptomic analysis of Alzheimer's disease. Nature 570:332–337. https://doi.org/10.1038/s41586-019-1195-2
54. Mathys H, Peng Z, Boix CA, Victor MB, Leary N, Babu S, Abdelhady G, Jiang X, Ng AP, Ghafari K, Kunisky AK, Mantero J, Galani K, Lohia VN, Fortier GE, Lotfi Y, Ivey J, Brown HP, Patel PR, Chakraborty N, Beaudway JI, Imhoff EJ, Keeler CF, McChesney MM, Patel HH, Patel SP, Thai MT, Bennett DA, Kellis M, Tsai L-H (2023) Single-cell atlas reveals correlates of high cognitive function, dementia, and resilience to Alzheimer's disease pathology. Cell 186:4365-4385.e27. https://doi.org/10.1016/j.cell.2023.08.039
55. McDavid A, Finak G, Chattopadyay PK, Dominguez M, Lamoreaux L, Ma SS, Roederer M, Gottardo R (2013) Data exploration, quality control and testing in single-cell qPCR-based gene expression experiments. Bioinformatics 29:461–467. https://doi.org/10.1093/bioinformatics/bts714
56. Mirbaha H, Holmes BB, Sanders DW, Bieschke J, Diamond MI (2015) Tau trimers are the minimal propagation unit spontaneously internalized to seed intracellular aggregation*. J Biol Chem 290:14893–14903. https://doi.org/10.1074/jbc.m115.652693
57. Morrison JH, Hof PR (2002) Chapter 37 Selective vulnerability of corticocortical and hippocampal circuits in aging and Alzheimer's disease. Prog Brain Res 136:467–486. https://doi.org/10.1016/s0079-6123(02)36039-4
58. Mudher A, Colin M, Dujardin S, Medina M, Dewachter I, Naini SMA, Mandelkow E-M, Mandelkow E, Buée L, Goedert M, Brion J-P (2017) What is the evidence that tau pathology spreads through prion-like propagation? Acta Neuropathol Commun 5:99. https://doi.org/10.1186/s40478-017-0488-7
59. Muñoz SS, Engel M, Balez R, Do-Ha D, Cabral-da-Silva MC, Hernández D, Berg T, Fifita JA, Grima N, Yang S, Blair IP, Nicholson G, Cook AL, Hewitt AW, Pébay A, Ooi L (2020) A simple differentiation protocol for generation of induced pluripotent stem cell-derived basal forebrain-like cholinergic neurons for alzheimer's disease and frontotemporal dementia disease modeling. Cells 9:2018. https://doi.org/10.3390/cells9092018
60. Muratore CR, Rice HC, Srikanth P, Callahan DG, Shin T, Benjamin LNP, Walsh DM, Selkoe DJ, Young-Pearse TL (2014) The familial Alzheimer's disease APPV717I mutation alters APP processing and Tau expression in iPSC-derived neurons. Hum Mol Genet 23:3523–3536. https://doi.org/10.1093/hmg/ddu064
61. Muratore CR, Zhou C, Liao M, Fernandez MA, Taylor WM, Lagomarsino VN, Pearse RV, Rice HC, Negri JM, He A, Srikanth P, Callahan DG, Shin T, Zhou M, Bennett DA, Noggle S, Love JC, Selkoe DJ, Young-Pearse TL (2017) Cell-type dependent alzheimer's disease phenotypes: probing the biology of selective neuronal vulnerability. Stem Cell Rep 9:1868–1884. https://doi.org/10.1016/j.stemcr.2017.10.015
62. Murdock MH, Tsai L-H (2023) Insights into Alzheimer's disease from single-cell genomic approaches. Nat Neurosci 26:181–195. https://doi.org/10.1038/s41593-022-01222-2
63. Nelson PT, Alafuzoff I, Bigio EH, Bouras C, Braak H, Cairns NJ, Castellani RJ, Crain BJ, Davies P, Tredici KD, Duyckaerts C, Frosch MP, Haroutunian V, Hof PR, Hulette CM, Hyman BT, Iwatsubo T, Jellinger KA, Jicha GA, Kövari E, Kukull WA, Leverenz JB, Love S, Mackenzie IR, Mann DM, Masliah E, McKee AC, Montine TJ, Morris JC, Schneider JA, Sonnen JA, Thal DR, Trojanowski JQ, Troncoso JC, Wisniewski T, Woltjer RL, Beach TG (2012) Correlation of alzheimer disease neuropathologic changes with cognitive status: a review of the literature. J Neuropathol Exp Neurol 71:362–381. https://doi.org/10.1097/nen.0b013e31825018f7
64. Otero-Garcia M, Mahajani SU, Wakhloo D, Tang W, Xue Y-Q, Morabito S, Pan J, Oberhauser J, Madira AE, Shakouri T, Deng Y, Allison T, He Z, Lowry WE, Kawaguchi R, Swarup V, Cobos I (2022) Molecular signatures underlying neurofibrillary tangle susceptibility in alzheimer's disease. Neuron 110:2929-2948.e8. https://doi.org/10.1016/j.neuron.2022.06.021
65. Polinski NK, Volpicelli-Daley LA, Sortwell CE, Luk KC, Cremades N, Gottler LM, Froula J, Duffy MF, Lee VM, Martinez TN, Dave KD (2018) Best practices for generating and using alpha-synuclein pre-formed fibrils to model parkinson's disease in rodents. J Park's Dis. https://doi.org/10.3233/jpd-171248
66. Pooler AM, Noble W, Hanger DP (2014) A role for tau at the synapse in alzheimer's disease pathogenesis. Neuropharmacology 76:1–8. https://doi.org/10.1016/j.neuropharm.2013.09.018
67. Rissman RA, Poon WW, Blurton-Jones M, Oddo S, Torp R, Vitek MP, LaFerla FM, Rohn TT, Cotman CW (2004) Caspase-cleavage of tau is an early event in Alzheimer disease tangle pathology. J Clin Investig 114:121–130. https://doi.org/10.1172/jci20640
68. Robbins M, Clayton E, Schierle GSK (2021) Synaptic Tau: a pathological or physiological phenomenon? Acta Neuropathol Commun 9:149. https://doi.org/10.1186/s40478-021-01246-y
69. Sakanaka M, Magari S, Inoue N (1990) Somatostatin co-localizes with tyrosine hydroxylase in the nerve cells of discrete hypothalamic regions in rats. Brain Res 516:313–317. https://doi.org/10.1016/0006-8993(90)90933-3
70. Satija R, Farrell JA, Gennert D, Schier AF, Regev A (2015) Spatial reconstruction of single-cell gene expression data. Nat Biotechnol 33:495–502. https://doi.org/10.1038/nbt.3192
71. Sato T, Imaizumi K, Watanabe H, Ishikawa M, Okano H (2021) Generation of region-specific and high-purity neurons from human feeder-free iPSCs. Neurosci Lett 746:135676. https://doi.org/10.1016/j.neulet.2021.135676
72. Schlegel K, Awwad K, Heym RG, Holzinger D, Doell A, Barghorn S, Jahn TR, Klein C, Mordashova Y, Schulz M, Gasparini L (2019) N368-Tau fragments generated by legumain are detected only in trace amount in the insoluble Tau aggregates isolated from AD brain. Acta Neuropathol Commun 7:177. https://doi.org/10.1186/s40478-019-0831-2
73. Schöndorf DC, Elschami M, Schieck M, Ercan-Herbst E, Weber C, Riesinger Y, Kalman S, Steinemann D, Ehrnhoefer DE (2019) Generation of an induced pluripotent stem cell cohort suitable to investigate sporadic Alzheimer's Disease. Stem Cell Res 34:101351. https://doi.org/10.1016/j.scr.2018.11.012
74. Smits LM, Reinhardt L, Reinhardt P, Glatza M, Monzel AS, Stanslowsky N, Rosato-Siri MD, Zanon A, Antony PM, Bellmann J, Nicklas SM, Hemmer K, Qing X, Berger E, Kalmbach N, Ehrlich M, Bolognin S, Hicks AA, Wegner F, Sterneckert JL, Schwamborn JC (2019) Modeling parkinson's disease in midbrain-like organoids. npj Park's Dis 5:5. https://doi.org/10.1038/s41531-019-0078-4
75. Stuart T, Butler A, Hoffman P, Hafemeister C, Papalexi E, Mauck WM, Hao Y, Stoeckius M, Smibert P, Satija R (2019) Comprehensive integration of single-cell data. Cell 177:1888-1902.e21. https://doi.org/10.1016/j.cell.2019.05.031
76. Surmeier DJ, Obeso JA, Halliday GM (2017) Selective neuronal vulnerability in parkinson disease. Nat Rev Neurosci 18:101–113. https://doi.org/10.1038/nrn.2016.178
77. Tao Y, Zhang S-C (2016) Neural subtype specification from human pluripotent stem cells. Cell Stem Cell 19:573–586. https://doi.org/10.1016/j.stem.2016.10.015
78. Tuck BJ, Miller LVC, Katsinelos T, Smith AE, Wilson EL, Keeling S, Cheng S, Vaysburd MJ, Knox C, Tredgett L, Metzakopian E, James LC, McEwan WA (2022) Cholesterol determines the cytosolic entry and seeded aggregation of tau. Cell Rep 39:110776. https://doi.org/10.1016/j.celrep.2022.110776
79. Vanlandingham PA, Ceresa BP (2009) Rab7 regulates late endocytic trafficking downstream of multivesicular body biogenesis and cargo sequestration*. J Biol Chem 284:12110–12124. https://doi.org/10.1074/jbc.m809277200
80. Vera E, Studer L (2015) When rejuvenation is a problem: challenges of modeling late-onset neurodegenerative disease. Development 142:3085–3089. https://doi.org/10.1242/dev.120667
81. Vitelli R, Santillo M, Lattero D, Chiariello M, Bifulco M, Bruni CB, Bucci C (1997) Role of the small GTPase RAB7 in the late endocytic pathway*. J Biol Chem 272:4391–4397. https://doi.org/10.1074/jbc.272.7.4391
82. Vogel JW, Iturria-Medina Y, Strandberg OT, Smith R, Levitis E, Evans AC, Hansson O, Weiner M, Aisen P, Petersen R, Jack CR, Jagust W, Trojanowki JQ, Toga AW, Beckett L, Green RC, Saykin AJ, Morris J, Shaw LM, Liu E, Montine T, Thomas RG, Donohue M, Walter S, Gessert D, Sather T, Jiminez G, Harvey D, Donohue M, Bernstein M, Fox N, Thompson P, Schuff N, DeCArli C, Borowski B, Gunter J, Senjem M, Vemuri P, Jones D, Kantarci K, Ward C, Koeppe RA, Foster N, Reiman EM, Chen K, Mathis C, Landau S, Cairns NJ, Householder E, Reinwald LT, Lee V, Korecka M, Figurski M, Crawford K, Neu S, Foroud TM, Potkin S, Shen L, Kelley F, Kim S, Nho K, Kachaturian Z, Frank R, Snyder PJ, Molchan S, Kaye J, Quinn J, Lind B, Carter R, Dolen S, Schneider LS, Pawluczyk S, Beccera M, Teodoro L, Spann BM, Brewer J, Vanderswag H, Fleisher A, Heidebrink JL, Lord JL, Petersen R, Mason SS, Albers CS, Knopman D, Johnson K, Doody RS, Meyer JV,

Chowdhury M, Rountree S, Dang M, Stern Y, Honig LS, Bell KL, Ances B, Morris JC, Carroll M, Leon S, Householder E, Mintun MA, Schneider S, OliverNG A, Griffith R, Clark D, Geldmacher D, Brockington J, Roberson E, Grossman H, Mitsis E, Toledo-Morrell L de, Shah RC, Duara R, Varon D, Greig MT, Roberts P, Albert M, Onyike C, D'Agostino D, Kielb S, Galvin JE, Pogorelec DM, Cerbone B, Michel CA, Rusinek H, Leon MJ de, Glodzik L, Santi SD, Doraiswamy PM, Petrella JR, Wong TZ, Arnold SE, Karlawish JH, Wolk D, Smith CD, Jicha G, Hardy P, Sinha P, Oates E, Conrad G, Lopez OL, Oakley M, Simpson DM, Porsteinsson AP, Goldstein BS, Martin K, Makino KM, Ismail MS, Brand C, Mulnard RA, Thai G, Ortiz CMA, Womack K, Mathews D, Quiceno M, Arrastia RD, King R, Weiner M, Cook KM, DeVous M, Levey AI, Lah JJ, Cellar JS, Burns JM, Anderson HS, Swerdlow RH, Apostolova L, Tingus K, Woo E, Silverman DHS, Lu PH, Bartzokis G, Radford NRG, Parfitt F, Kendall T, Johnson H, Farlow MR, Hake AM, Matthews BR, Herring S, Hunt C, Dyck CH van, Carson RE, MacAvoy MG, Chertkow H, Bergman H, Hosein C, Black S, Stefanovic B, Caldwell C, Hsiung GYR, Feldman H, Mudge B, Past MA, Kertesz A, Rogers J, Trost D, Bernick C, Munic D, Kerwin D, Mesulam MM, Lipowski K, Wu CK, Johnson N, Sadowsky C, Martinez W, Villena T, Turner RS, Johnson K, Reynolds B, Sperling RA, Johnson KA, Marshall G, Frey M, Yesavage J, Taylor JL, Lane B, Rosen A, Tinklenberg J, Sabbagh MN, Belden CM, Jacobson SA, Sirrel SA, Kowall N, Killiany R, Budson AE, Norbash A, Johnson PL, Obisesan TO, Wolday S, Allard J, Lerner A, Ogrocki P, Hudson L, Fletcher E, Carmichael O, Olichney J, DeCarli C, Kittur S, Borrie M, Lee TY, Bartha R, Johnson S, Asthana S, Carlsson CM, Potkin SG, Preda A, Nguyen D, Tariot P, Fleisher A, Reeder S, Bates V, Capote H, Rainka M, Scharre DW, Kataki M, Adeli A, Zimmerman EA, Celmins D, Brown AD, Pearlson GD, Blank K, Anderson K, Santulli RB, Kitzmiller TJ, Schwartz ES, SinkS KM, Williamson JD, Garg P, Watkins F, Ott BR, Querfurth H, Tremont G, Salloway S, Malloy P, Correia S, Rosen HJ, Miller BL, Mintzer J, Spicer K, Bachman D, Finger E, Pasternak S, Rachinsky I, Rogers J, Kertesz A, Drost D, Pomara N, Hernando R, Sarrael A, Schultz SK, Ponto LLB, Shim H, Smith KE, Relkin N, Chaing G, Raudin L, Smith A, Fargher K, Raj BA, Andersson E, Berron D, Byman E, Sundberg-Brorsson T, Administrator, Borland E, Callmer A, Dahl C, Gertje E, Gustavsson A-M, Grzegorska J, Hall S, Hansson O, Insel P, Janelidze S, Johansson M, Sletten H, Jester-Broms J, Londos E, Mattson N, Minthon L, Nilsson M, Nordkvist R, Nägga K, Orbjörn C, Ossenkoppele R, Palmqvist S, Persson M, Santillo A, Spotorno N, Stomrud E, Toresson H, Strandberg O, Schöll M, Friberg I, Johansson P, Wibom M, Johansson K, Pettersson E, Karremo C, Smith R, Surova Y, Jalakas M, Lätt J, Mannfolk P, Nilsson M, Ståhlberg F, Sundgren P, Westen D van, Andreasson U, Blennow K, Zetterberg H, Wahlund L-O, Westman E, Pereira J, Jögi J, Hägerström D, Olsson T, Wollmer P (2020) Spread of pathological tau proteins through communicating neurons in human Alzheimer's disease. Nat Commun 11: 2612

83. Vogel JW, Young AL, Oxtoby NP, Smith R, Ossenkoppele R, Strandberg OT, Joie RL, Aksman LM, Grothe MJ, Iturria-Medina Y, Weiner M, Aisen P, Petersen R, Jack CR, Jagust W, Trojanowki JQ, Toga AW, Beckett L, Green RC, Saykin AJ, Morris J, Shaw LM, Liu E, Montine T, Thomas RG, Donohue M, Walter S, Gessert D, Sather T, Jiminez G, Harvey D, Bernstein M, Fox N, Thompson P, Schuff N, DeCArli C, Borowski B, Gunter J, Senjem M, Vemuri P, Jones D, Kantarci K, Ward C, Koeppe RA, Foster N, Reiman EM, Chen K, Mathis C, Landau S, Cairns NJ, Householder E, Reinwald LT, Lee V, Korecka M, Figurski M, Crawford K, Neu S, Foroud TM, Potkin S, Shen L, Kelley F, Kim S, Nho K, Kachaturian Z, Frank R, Snyder PJ, Molchan S, Kaye J, Quinn J, Lind B, Carter R, Dolen S, Schneider LS, Pawluczyk S, Beccera M, Teodoro L, Spann BM, Brewer J, Vanderswag H, Fleisher A, Heidebrink JL, Lord JL, Mason SS, Albers CS, Knopman D, Johnson K, Doody RS, Meyer JV, Chowdhury M, Rountree S, Dang M, Stern Y, Honig LS, Bell KL, Ances B, Morris JC, Carroll M, Leon S, Mintun MA, Schneider S, Oliver A, Griffith R, Clark D, Geldmacher D, Brockington J, Roberson E, Grossman H, Mitsis E, deToledo-Morrell L, Shah RC, Duara R, Varon D, Greig MT, Roberts P, Albert M, Onyike C, D'Agostino D, Kielb S, Galvin JE, Pogorelec DM, Cerbone B, Michel CA, Rusinek H, de Leon MJ, Glodzik L, Santi SD, Doraiswamy PM, Petrella JR, Wong TZ, Arnold SE, Karlawish JH, Wolk D, Smith CD, Jicha G, Hardy P, Sinha P, Oates E, Conrad G, Lopez OL, Oakley M, Simpson DM, Porsteinsson AP, Goldstein BS, Martin K, Makino KM, Ismail MS, Brand C, Mulnard RA, Thai G, Ortiz CM, Womack K, Mathews D, Quiceno M, Arrastia RD, King R, Weiner M, Cook KM, DeVous M, Levey AI, Lah JJ, Cellar JS, Burns JM, Anderson HS, Swerdlow RH, Apostolova L, Tingus K, Woo E, Silverman DHS, Lu PH, Bartzokis G, Radford NRG, Parfitt F, Kendall T, Johnson H, Farlow MR, Hake AM, Matthews BR, Herring S, Hunt C, van Dyck CH, Carson RE, MacAvoy MG, Chertkow H, Bergman H, Hosein C, Black S, Stefanovic B, Caldwell C, Hsiung GYR, Feldman H, Mudge B, Past MA, Kertesz A, Rogers J, Trost D, Bernick C, Munic D, Kerwin D, Mesulam MM, Lipowski K, Wu CK, Johnson N, Sadowsky C, Martinez W, Villena T, Turner RS, Johnson K, Reynolds B, Sperling RA, Johnson KA, Marshall G, Frey M, Yesavage J, Taylor JL, Lane B, Rosen A, Tinklenberg J, Sabbagh MN, Belden CM, Jacobson SA, Sirrel SA, Kowall N, Killiany R, Budson AE, Norbash A, Johnson PL, Obisesan TO, Wolday S, Allard J, Lerner A, Ogrocki P, Hudson L, Fletcher E, Carmichael O, Olichney J, DeCarli C, Kittur S, Borrie M, Lee TY, Bartha R, Johnson S, Asthana S, Carlsson CM, Potkin SG, Preda A, Nguyen D, Tariot P, Reeder S, Bates V, Capote H, Rainka M, Scharre DW, Kataki M, Adeli A, Zimmerman EA, Celmins D, Brown AD, Pearlson GD, Blank K, Anderson K, Santulli RB, Kitzmiller TJ, Schwartz ES, Sink KM, Williamson JD, Garg P, Watkins F, Ott BR, Querfurth H, Tremont G, Salloway S, Malloy P, Correia S, Rosen HJ, Miller BL, Mintzer J, Spicer K, Bachman D, Finger E, Pasternak S, Rachinsky I, Drost D, Pomara N, Hernando R, Sarrael A, Schultz SK, Ponto LLB, Shim H, Smith KE, Relkin N, Chaing G, Raudin L, Smith A, Fargher K, Raj BA, Pontecorvo MJ, Devous MD, Rabinovici GD, Alexander DC, Lyoo CH, Evans AC, Hansson O (2021) Four distinct trajectories of tau deposition identified in Alzheimer's disease. Nat Med 27:871–881. https://doi.org/10.1038/s41591-021-01309-6
84. Volpato V, Smith J, Sandor C, Ried JS, Baud A, Handel A, Newey SE, Wessely F, Attar M, Whiteley E, Chintawar S, Verheyen A, Barta T, Lako M, Armstrong L, Muschet C, Artati A, Cusulin C, Christensen K, Patsch C, Sharma E, Nicod J, Brownjohn P, Stubbs V, Heywood WE, Gissen P, Filippis RD, Janssen K, Reinhardt P, Adamski J, Royaux I, Peeters PJ, Terstappen GC, Graf M, Livesey FJ, Akerman CJ, Mills K, Bowden R, Nicholson G, Webber C, Cader MZ, Lakics V (2018) Reproducibility of molecular phenotypes after long-term differentiation to human iPSC-derived neurons: a multi-site omics study. Stem Cell Rep 11:897–911. https://doi.org/10.1016/j.stemcr.2018.08.013
85. Wischik CM, Novak M, Thøgersen HC, Edwards PC, Runswick MJ, Jakes R, Walker JE, Milstein C, Roth M, Klug A (1988) Isolation of a fragment of tau derived from the core of the paired helical filament of Alzheimer disease. Proc Natl Acad Sci 85:4506–4510. https://doi.org/10.1073/pnas.85.12.4506
86. Wu JW, Herman M, Liu L, Simoes S, Acker CM, Figueroa H, Steinberg JI, Margittai M, Kayed R, Zurzolo C, Paolo GD, Duff KE (2013) Small misfolded tau species are internalized via bulk endocytosis and anterogradely and retrogradely transported in neurons*. J Biol Chem 288:1856–1870. https://doi.org/10.1074/jbc.m112.394528
87. Wu JW, Hussaini SA, Bastille IM, Rodriguez GA, Mrejeru A, Rilett K, Sanders DW, Cook C, Fu H, Boonen RACM, Herman M, Nahmani E, Emrani S, Figueroa YH, Diamond MI, Clelland CL, Wray S, Duff KE (2016) Neuronal activity enhances tau propagation and tau pathology in vivo. Nat Neurosci 19:1085–1092. https://doi.org/10.1038/nn.4328
88. Wu T, Hu E, Xu S, Chen M, Guo P, Dai Z, Feng T, Zhou L, Tang W, Zhan L, Fu X, Liu S, Bo X, Yu G (2021) clusterProfiler 4.0: a universal enrichment tool for interpreting omics data. Innovation 2:100141. https://doi.org/10.1016/j.xinn.2021.100141
89. Yap CC, Digilio L, McMahon LP, Garcia ADR, Winckler B (2018) Degradation of dendritic cargos requires Rab7-dependent transport to somatic lysosomes. J Cell Biol 217:3141–3159. https://doi.org/10.1083/jcb.201711039
90. Yu G, Wang L-G, Han Y, He Q-Y (2012) clusterProfiler: an R package for comparing biological themes among gene clusters. Omics J Integr Biol 16:284–287. https://doi.org/10.1089/omi.2011.0118
91. Zhang Z, Song M, Liu X, Kang SS, Kwon I-S, Duong DM, Seyfried NT, Hu WT, Liu Z, Wang J-Z, Cheng L, Sun YE, Yu SP, Levey AI, Ye K (2014) Cleavage of tau by asparagine endopeptidase mediates the neurofibrillary pathology in Alzheimer's disease. Nat Med 20:1254–1262. https://doi.org/10.1038/nm.3700

Publisher's Note